Computer Modeling in
Engineering & Sciences

Tech Science Press

https://doi.org/10.32604/cmes.2026.087251

REVIEW

From Lattice Boltzmann Acoustics to Quantum Lattice Boltzmann Methods: A Physics-Guided Roadmap for Quantum Flow Simulations

Muhammad Idrees Khan* **and Hua-Dong Yao**

Department of Mechanical Engineering, Chalmers University of Technology, Gothenburg, Sweden

*Corresponding Author: Muhammad Idrees Khan. Email: idreesm@chalmers.se

Received: 12 June 2026; Accepted: 04 August 2026; Published: 28 August 2026

ABSTRACT: Quantum computational fluid dynamics (QCFD) is an active but still immature research area, and quantum lattice Boltzmann methods (QLBM) provide a natural mesoscopic route because their collision–streaming structure can be decomposed into algorithmic blocks. This paper reviews QLBM and related hybrid quantum–classical fluid approaches from an engineering computational fluid dynamics (CFD) perspective, emphasizing physical scope, boundary realism, nonlinear collision treatment, measurement cost, hardware assumptions, and comparison with optimized classical baselines. The discussion is connected to computational aeroacoustics (CAA), where practical workflows already separate source generation, acoustic propagation, and design loops, creating possible insertion points for selective quantum or hybrid acceleration. As a concrete classical reference problem, we also develop a three-dimensional, 19-velocity (D3Q19) multiple-relaxation-time (MRT) lattice Boltzmann method (LBM) acoustic benchmark. In this benchmark, harmonic monopole, dipole, and quadrupole sources are imposed through an additive particle source term, and the computed fields are validated against a D3Q19 MRT-specific Chapman–Enskog macroscopic reference derived from the implemented collision model and source moments using axial waveforms and far-field directivity. The same benchmark is then mapped to an illustrative QLBM architecture using Carleman lifting, linear combination of unitaries (LCU) or block encoding, conditional streaming, and acoustic readout. The resulting roadmap argues that near- and mid-term quantum contributions to aeroacoustics are more likely to appear through targeted hybrid kernels and benchmarked mesoscopic subproblems, rather than replacing mature industrial CFD/CAA pipelines.

KEYWORDS: Quantum lattice Boltzmann method; quantum computational fluid dynamics; computational aeroacoustics; lattice Boltzmann method; hybrid quantum–classical algorithms; multiple-relaxation-time LBM; acoustic multipole sources; Carleman lifting

1 Introduction

This review situates quantum lattice Boltzmann methods (QLBM), defined here as quantum algorithms involving circuits, encodings, and measurements for fluid-dynamics problems expressed through lattice Boltzmann formulations, within the broader field of quantum computational fluid dynamics (QCFD). Within this broad field, partial differential equation (PDE) formulations, Navier–Stokes (NS)-oriented quantum routes, quantum machine learning (QML), quantum-inspired approaches, hybrid linear solvers, and mesoscopic methods appear as recurring algorithmic families. The discussion is organized around major themes and application-driven questions. Tables 1–6 summarize the benchmark ladder, baseline comparisons, representative QLBM literature, acoustic-observable templates, and engineering-readiness mapping.

Literature Search Strategy and Review Organization

The review was designed as a structured critical and scoping review rather than a formal meta-analysis or pooled-effect systematic review. The strategy follows guidance for literature reviews and scoping studies, while using Preferred Reporting Items for Systematic Reviews and Meta-Analyses (PRISMA)-informed reporting principles to make the search and screening process systematic [1–4]. Searches were performed in Web of Science, Scopus, Google Scholar, IEEE Xplore, arXiv, AIAA, Springer, Elsevier, APS, ACM, and publisher databases. Search terms included "quantum lattice Boltzmann", "quantum computational fluid dynamics", "quantum Navier–Stokes", "quantum advection–diffusion", "hybrid quantum classical computational fluid dynamics (CFD)", "quantum linear solver fluid dynamics", "Carleman quantum fluid", "lattice Boltzmann acoustics", "LBM aeroacoustics", "absorbing layers lattice Boltzmann method (LBM)", "computational aeroacoustics fan noise", and "Helmholtz liner acoustics".

Papers were retained if they contributed to QLBM, broader QCFD, quantum PDE algorithms, hybrid quantum linear solvers for flow or acoustics, classical LBM foundations, large-eddy simulation (LBM-LES), LBM aeroacoustics, or computational aeroacoustics (CAA) workflows relevant to aeroacoustic observables. Papers were excluded if the term "quantum lattice Boltzmann" referred only to classical solvers for quantum kinetic equations without relevance to quantum computing, or if the work lacked any connection to fluid simulation, acoustic observables, or computational modeling. The final corpus was grouped into eight categories, covering QCFD surveys, QLBM algorithms, quantum PDE/linear solvers, quantum-inspired/QML CFD, classical LBM and LBM-LES, LBM acoustics, CAA and rotating-machinery acoustics, and resource-estimation/measurement literature. The database list, search strings, eligibility criteria, exclusion criteria, and citation-expansion steps are reported to provide a clear account of how the review corpus was assembled [5]. In the audit log, 1173 raw hits were recorded for transparency, 822 records were entered into the screening table, 284 duplicate records were removed, and 538 unique records remained after deduplication. Manual title/abstract screening excluded 424 records and retained 114 records for corpus checking. Broad raw-hit counts were not treated as screened records unless individual records were exported or entered into the screening log. The current manuscript reference list contains 171 references; the audit was used to reconcile this bibliography against screened records and to identify additional candidate papers as part of a retrospective transparency step rather than a prospectively registered systematic-review protocol. Fig. 1 summarizes the retrospective PRISMA-informed search-audit workflow used to document record identification, deduplication, manual title/abstract screening, and bibliography reconciliation.

The review draws on peer-reviewed articles and identifiable preprints published through July 2026 on quantum and hybrid fluid algorithms, with QLBM as the central focus. It also uses classical LBM and computational aeroacoustics literature to provide comparison, validation context, and application framing. Because the objective is to map an emerging interdisciplinary field rather than estimate a pooled effect size, the review should be interpreted as a structured critical and scoping review with a descriptive bibliometric component [1,2,6]. Propellers, fans, and installed propulsion serve as representative application touchpoints for computational aeroacoustics, where flow simulation is coupled with sound prediction and design.

CFD is standard in aerospace, energy, transport, and turbomachinery, yet high-fidelity prediction remains costly when turbulence, moving boundaries, flow–acoustic coupling, and repeated design loops must all be resolved. In aeroacoustics and rotating machinery, the structures that generate sound are often weak but sensitive to how unsteadiness is resolved.

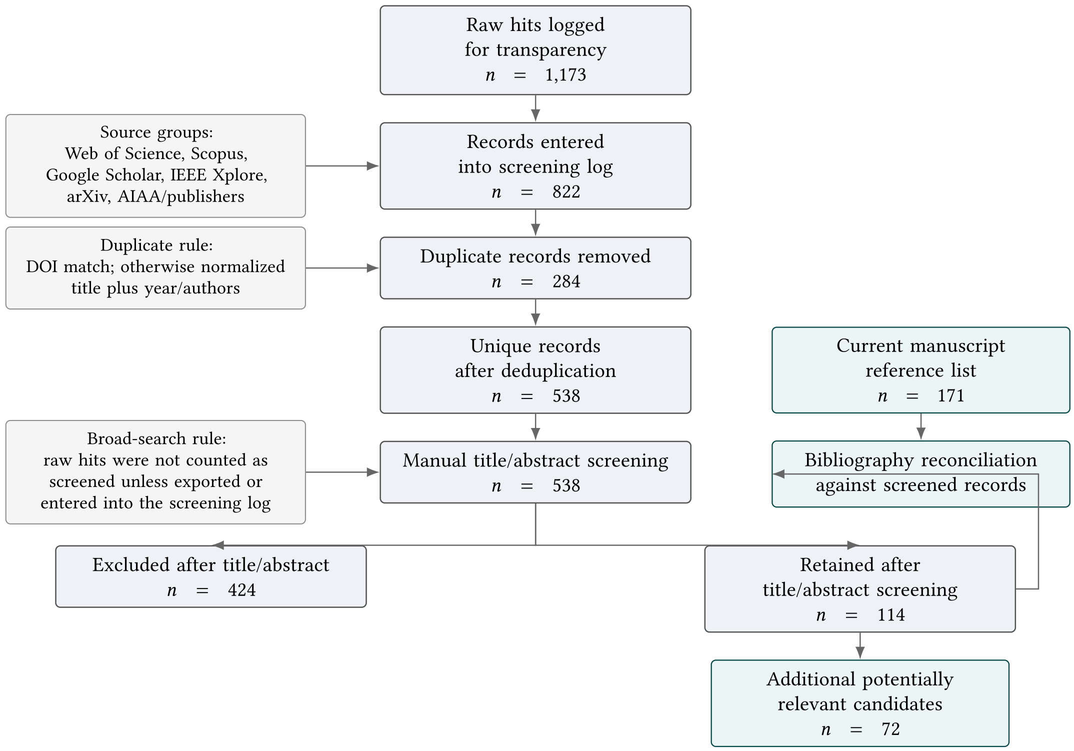

Figure 1: Retrospective Preferred Reporting Items for Systematic Reviews and Meta-Analyses (PRISMA)-informed search audit and bibliography-reconciliation workflow. Raw database hits were logged for transparency but were not counted as screened unless exported or recorded into the screening table. Duplicate records were removed by digital object identifier (DOI) where available and otherwise by normalized title, year, and authorship metadata. Manual title/abstract screening was used to retain records relevant to quantum lattice Boltzmann methods (QLBM), quantum computational fluid dynamics (QCFD), quantum partial differential equation (PDE) and linear solvers, hybrid CFD and CAA kernels, classical lattice Boltzmann method (LBM), large-eddy simulation (LES), LBM-LES, LBM acoustics, CAA workflows, and resource/measurement literature.

Industrial CAA is commonly organized around flow simulation, source extraction, acoustic propagation, and design iteration. This decomposition provides natural entry points for discussing hybrid or quantum-assisted methods, without requiring the assumption of a single end-to-end quantum flow solver.

Quantum algorithms have attracted growing interest for fluid-related problems, but fluid dynamics remains nonlinear, multiscale, and difficult to measure on quantum hardware in full generality [7–9]. QLBM is a useful focal point because its collision–streaming structure aligns closely with the way classical LBM and CFD are already formulated and discussed. Broad QCFD reviews map algorithmic families and hardware horizons [7,8], while related surveys examine quantum machine learning and quantum-inspired approaches for CFD [9]. Aerospace-oriented studies have also explored variational quantum algorithms on model flow problems [10]. Building on this context, the present review emphasizes QLBM and connects it to classical LBM–LES foundations (Section 3.5), evaluation criteria and CAA-oriented benchmarks (Sections 6 and 7), linear-acoustics interfaces (Section 8), and the research roadmap (Section 12).

In parts of the mathematical-physics literature, the phrase "quantum lattice Boltzmann" can denote a classical lattice Boltzmann–type discretization used to approximate quantum kinetic or master equations. In this usage, it is a classical numerical scheme for quantum equations. In the quantum-computing literature, QLBM refers to quantum algorithms, including circuits, encodings, and measurements, aimed at fluid-dynamics problems. This review uses QLBM only in the latter sense. Where a collision–streaming update is meant generically, we write "LBM-like" or "mesoscopic step" to keep the two usages distinct.

Within this broad field, LBM warrants sustained attention. Monographs and textbooks document classical formulation, validation practice, and implementation [11,12]. Classical LBM is already well known for its regular data structures, locality, complex-boundary handling, and strong performance on parallel architectures. It has also become a valuable tool for weakly compressible turbulence, multiphase transport, porous-media flow, and selected aeroacoustic workflows. These properties make LBM an attractive candidate as a conceptual bridge to quantum computing. The discrete collision–streaming structure lends itself to algorithmic decomposition, while the mesoscopic state representation opens alternative encoding strategies that differ from direct discretizations of the Navier–Stokes equations. For this reason, QLBM has attracted substantial research activity within QCFD [13–17].

The scope of this review assumes that QLBM will complement direct numerical simulation (DNS), LES, and hybrid CFD/CAA workflows in the near term. This perspective is motivated by low-noise propulsion and engineering aeroacoustics, including sound prediction for propellers and fans [18,19]. Source-based CAA commonly builds on Lighthill's acoustic analogy and its extension to moving surfaces through the Ffowcs Williams–Hawkings formulation [20,21]. These source formulations are coupled with acoustic-propagation models and evaluated using receiver-side quantities such as spectra, directivity, and sound-pressure levels [22,23].

The scope stays close to QLBM and hybrid routes for aeroacoustic and low-noise propulsion needs, while whole-field QCFD surveys supply orientation and context [7,8]. Concrete entry points, including transport kernels, linear subproblems, and outer-loop tasks, are spelled out where they sharpen the discussion.

The paper also introduces a compact classical multiple-relaxation-time (MRT) lattice Boltzmann method (LBM) acoustic benchmark, together with an illustrative quantum-compatible reformulation of the same algorithmic structure. Harmonic monopole, dipole, and quadrupole sources are generated at the population level by an additive particle source term and propagated in a quiescent weakly compressible lattice. The source-moment idea is related to earlier LBM multipole work [24], but the analytical reference used here is derived directly for the implemented D3Q19 MRT scheme. The resulting axial pressure waveforms and far-field directivity patterns are compared with an MRT-derived Chapman–Enskog (CE) macroscopic point-source reference. The benchmark establishes a classical acoustic reference problem. The subsequent QLBM-oriented reformulation maps the same update to a mainstream lifted-operator architecture using Carleman linearization, linear combination of unitaries (LCU) or block encoding, conditional streaming, and acoustic readout. Fig. 2 shows how the review narrows from QCFD to QLBM and then to aeroacoustic motivation.

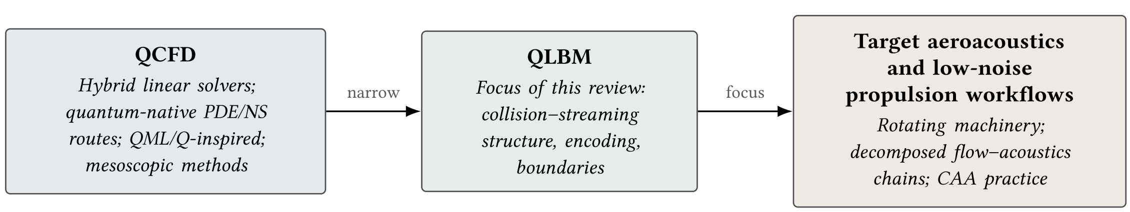

Figure 2: Structure of the review, from the broad QCFD landscape, including quantum-native partial differential equation/Navier–Stokes (NS) routes, quantum machine learning (QML), and quantum-inspired (Q-inspired) routes, to QLBM as the methodological emphasis and then to target aeroacoustic and low-noise propulsion workflows (right-hand box). QCFD remains broader than QLBM alone.

2 Broad Quantum CFD Background

Early QCFD studies followed several distinct algorithmic routes. Ray et al. reformulated a reduced transient channel-flow problem as a binary optimization problem for adiabatic quantum annealing [25]. Griffin et al. examined universal-gate strategies for direct numerical simulation of the incompressible Navier–Stokes equations, emphasizing state encoding, nonlinear-term treatment, and readout limitations [26]. Gaitan proposed a quantum PDE algorithm and demonstrated it for quasi-one-dimensional compressible nozzle flows, while Oz et al. adapted this approach to Burgers' equation with and without shock formation [27,28].

Separately, the Harrow–Hassidim–Lloyd (HHL) algorithm established a foundational quantum linear-system method [29]. Subsequent hybrid quantum–classical CFD studies targeted specific components of classical solvers. Chen et al. proposed a quantum acceleration strategy for steady finite-volume CFD with explicit treatment of classical input and output [30]. Lapworth embedded HHL within a pressure–velocity-coupling hybrid CFD solver and reported lid-driven-cavity benchmarks [31]. Song et al. applied a variational quantum linear solver to the pressure-Poisson step of an incompressible projection method and tested the approach on noisy quantum hardware [32]. Chen et al. later introduced iterative quantum linear solving and subspace scaling, demonstrating Poiseuille flow and acoustic-wave propagation on superconducting hardware [33]. Bharadwaj and Sreenivasan developed QFlowS and demonstrated gate-level hybrid quantum linear-system workflows for low-Reynolds-number flows, including state-preparation and quantum post-processing considerations [34]. Other quantum-native fluid formulations include hydrodynamic Schrödinger reformulations, incompressible nonlinear Navier–Stokes algorithms, and potential quantum-advantage analyses for fluid dynamics [35–39].

For orientation, the QCFD literature can be grouped into four overlapping families [7,8]: hybrid quantum linear-solver approaches for discretized flow problems; quantum-native PDE and ensemble reformulations; QLBM [13,15,17,40]; and quantum machine learning or quantum-inspired approaches for CFD [9,41]. Recent work also broadens the QCFD landscape through general perspectives on quantum simulation of fluid flows [42], fully quantum lattice-based mesoscale algorithms demonstrated for diffusion and Burgers' equations [43], and particle-based quantum hydrodynamics formulations such as Smoothed Particle Hydrodynamics (SPH) [44]. Fig. 3 sketches this taxonomy. The remainder of the paper concentrates on QLBM and hybrid linear-acoustics interfaces, while broader QCFD coverage is left to the surveys cited above.

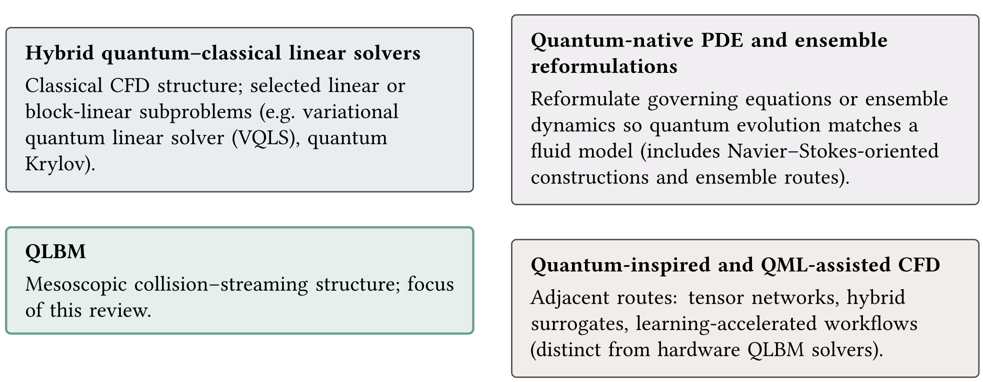

Figure 3: High-level taxonomy of QCFD, covering four overlapping families used in this review: hybrid quantum–classical linear-solver approaches for discretized flow problems, including variational quantum linear solver (VQLS) routes [30–33]; quantum-native PDE, Navier–Stokes-oriented, and ensemble reformulations [27,35,38,39]; QLBM [13,15,17,40]; and quantum machine learning or quantum-inspired CFD approaches [9,41]. QLBM is the methodological emphasis of this review.

Near-term fluid simulation is likely to use quantum methods on selected subproblems, such as sparse linear systems, outer-loop solves, or hybrid blocks in which turbulence remains on classical hardware [32,33]. Broader analyses of potential quantum advantage for fluid dynamics [37] address longer-horizon algorithmic possibilities beyond these hardware-grounded demonstrations. Fig. 4 summarizes the usual near-term, mid-term, and long-term layering [7–9].

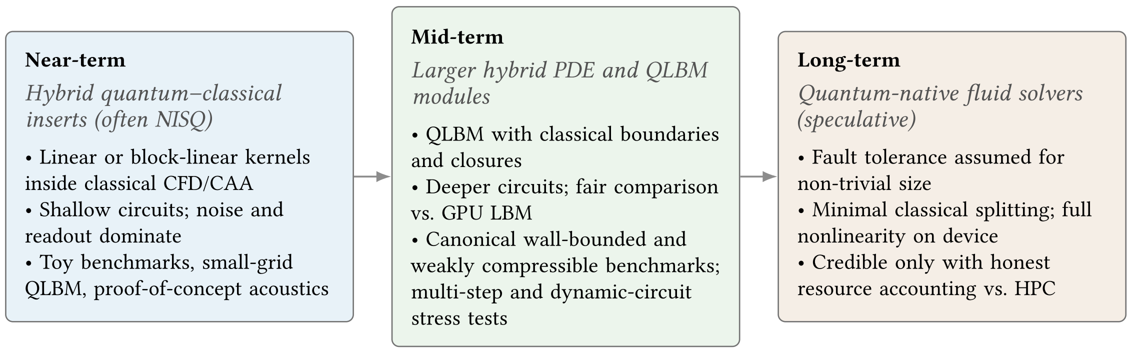

Figure 4: Schematic overview of near-, mid-, and long-term horizons for quantum CFD and QLBM, informed by broad QCFD and related quantum/quantum-inspired CFD literature reviews [7–9]. Here, noisy intermediate-scale quantum (NISQ), graphics processing unit (GPU), and high-performance computing (HPC) denote the hardware and computing contexts used in the figure. The bullets summarize the authors' synthesis of the landscape instead of direct quotations from a single source. Further details and caveats are discussed in the main text.

Critical Synthesis of QCFD Routes

The taxonomy in Fig. 3 assigns different maturity levels and engineering relevance to the QCFD branches. Hybrid quantum–classical linear-solver approaches are currently the most directly aligned with established CFD and CAA workflows because pressure-Poisson, Helmholtz, linearized Navier–Stokes, and other block-linear subproblems already appear inside classical solvers. At the algorithmic level, their potential advantage depends on efficient sparse-matrix access, conditioning or preconditioning, state preparation, and restricted output extraction [29,45,46]. CFD-oriented demonstrations additionally show that solver integration, hardware noise, and recovery of useful flow observables remain practical bottlenecks [30–33].

Quantum-native PDE and Navier–Stokes reformulations are more ambitious because they alter the mathematical representation of the governing equations. Early routes include annealing-based and nonlinear or unitary PDE formulations tested mainly on reduced or model flow problems [25,27,38]. Other proposals use hydrodynamic Schrödinger representations, ensemble formulations, or direct incompressible Navier–Stokes constructions [35,36,39]. These approaches are important as long-horizon algorithmic proposals, but their extension to wall-bounded, turbulent, geometry-dependent engineering flow remains to be established.

QLBM occupies a middle position. Its main strength is structural: collision, streaming, moment recovery, and boundary handling are already natural units of mesoscopic CFD algorithms. This makes QLBM easier to compare with classical LBM than direct quantum discretizations of the Navier–Stokes equations. Its main weakness is equally structural: the classical LBM steps most valuable for engineering (nonlinear equilibrium, dissipative collision, complex boundaries, forcing, turbulence closure, and repeated readout of fields or spectra) are precisely the steps that are hardest to implement coherently and economically on quantum hardware. Quantum-inspired and QML-assisted routes are therefore best viewed as adjacent accelerators or surrogates rather than substitutes for a validated quantum flow solver [9,41]. From an engineering perspective, the clearest near- and mid-term directions are bounded subproblems with local or low-dimensional outputs: linear acoustic propagation blocks, weakly compressible transport kernels, benchmarked QLBM collision–streaming modules, and design-loop components where the measurement target is explicit.

3 The Evolution of QLBM Literature

The reviewed QLBM and QCFD literature is strongly weighted toward recent work, especially during 2021–2026. Fig. 5 summarizes selected landmark contributions on a thematic timeline. The figure is intended as a curated map of the QCFD and QLBM literature, while the descriptive bibliometric component is limited to publication year and topic grouping [6]. The subsections below follow thematic branches instead of strict chronology.

Table 1: Suggested benchmark ladder for QCFD and QLBM research, proposed here as a qualitative synthesis aid based on the literature reviewed in this paper. The first rung covers linear advection-diffusion equation (ADE) or scalar-transport benchmarks. Higher rungs require stronger justification against optimized classical baselines and clearer boundary-condition realism.

Rung	Stage	Typical Content and Purpose
1	Linear ADE or scalar transport	Isolate encoding, collision, streaming, and measurement; establish consistency with LBM modified equations.
2	Poiseuille, Couette, and Couette-like shear	Basic validation of viscous physics and boundary treatment in simple flows.
3	Lid-driven cavity benchmarks	Standard incompressible-flow diagnostics; still far from industrial turbulence.
4	Weakly compressible and mesoscopic transport-acoustics	LBM-native weakly compressible flow, acoustic-relevant transport, and mesoscopic sound-generation settings; bridge toward strengths of the mesoscopic picture.
5	Linearized acoustics and wave propagation	Helmholtz, linearized Navier–Stokes, and related wave-propagation subproblems aligned with hybrid QCFD linear solvers, including frequency-domain or outer-loop acoustics blocks.
6	Homogeneous and decaying turbulence snippets	Stress-test nonlinearity and resolution scaling below wall-bounded LES.
7	Engineering aeroacoustics and rotating machinery	Coupled flow, acoustics, and geometry variation; comparisons become meaningful only after lower rungs are satisfied.

Because the field is still young, recency alone is a poor proxy for importance. In the discussion below, a contribution is treated as a landmark when it changes the algorithmic bottleneck being addressed, the physical regime being attempted, or the validation standard expected of later work. Incremental developments remain valuable when they reduce overhead, clarify consistency, or improve implementation realism, yet landmark methods that open a new class of QLBM test problems carry greater weight in this review. This distinction is used below to separate four questions that are often conflated: whether a method is physically more expressive, whether it is more resource efficient, whether it improves time-marching or boundary realism, and whether it produces observables that a CFD or CAA user would actually need.

The comparison below also separates the physical equation being targeted, the quantum representation used for collision and streaming, the numerical or benchmark evidence reported, and the extent of resource accounting. Reported accuracy, qubit counts, gate counts, circuit depth, ancilla requirements, and measurement costs are noted in Table 3 where the cited studies provide them. Many current works still offer only partial resource estimates or proof-of-concept circuit demonstrations, which limits direct engineering comparison with optimized classical LBM from a CFD/CAA perspective. For this reason, Table 3 treats resource reporting itself as part of the critical assessment. When a study reports qubit counts, gate counts, circuit depth, benchmark errors, or measurement requirements, these are identified at the level reported in the cited work. When such information is absent or only partially specified, the table states this explicitly. This avoids treating all QLBM papers as equally mature and makes clear which contributions are algorithmic proposals, which are benchmark demonstrations, and which already include engineering-relevant resource accounting.

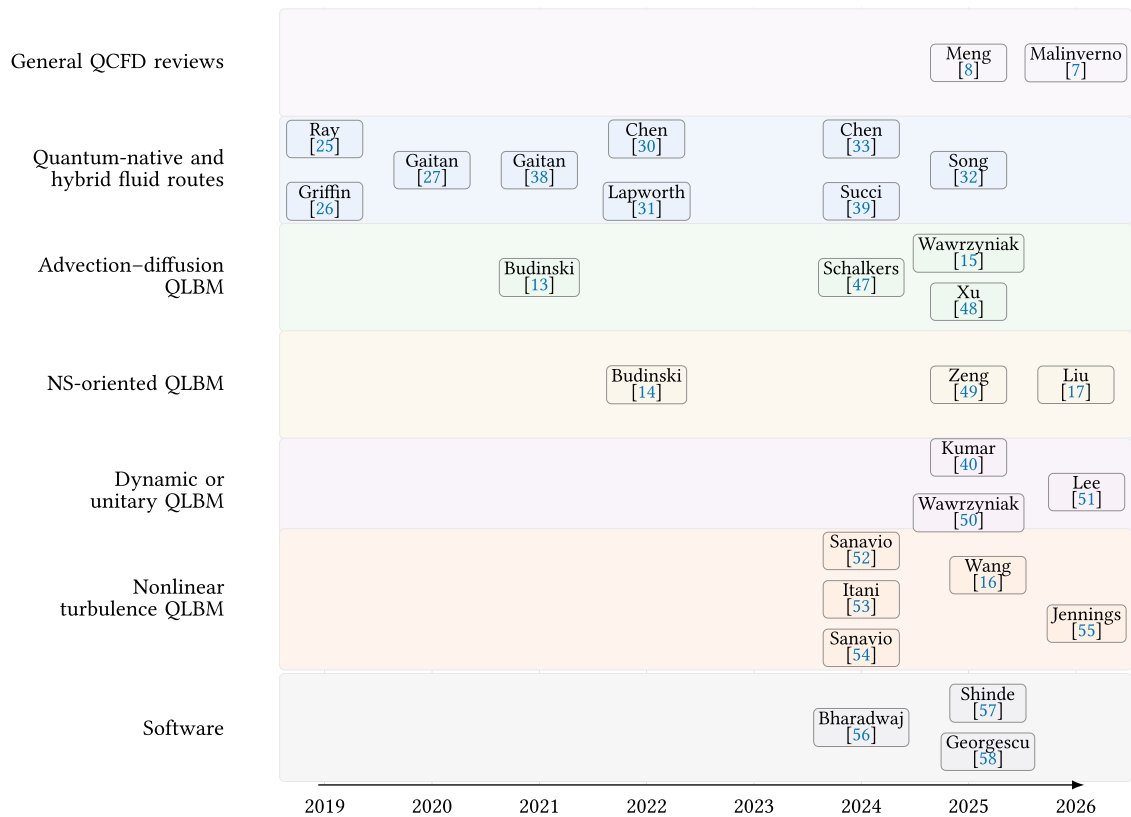

Figure 5: Selected landmark timeline for QCFD and QLBM literature, organized by publication year and theme. Marker labels show first-author surname and reference number. Horizontal position indicates calendar year, row tint indicates theme, and vertically stacked markers denote distinct works from the same year within a row. References: [7,8,13–17,25–27,30–33,38–40,47–58].

3.1 Early Linear Transport and Advection–Diffusion Formulations

Earlier quantum lattice-gas CFD work provides a useful historical antecedent to modern QLBM formulations, even though the present review uses QLBM in the quantum-computing algorithmic sense rather than as a classical solver for quantum kinetic equations [59].

An early QLBM study by Budinski formulated the advection–diffusion equation (ADE) within an LBM framework and presented a collision–streaming style quantum update pipeline [13]. The key idea was to exploit the LBM update structure to obtain a quantum algorithm composed of initialization, collision, propagation, and measurement steps. The work helped establish a recognizable template for later QLBM research, beginning with linear or linearized physics, careful attention to mesoscopic population encoding, and explicit treatment of multiple time steps.

The later work by Wawrzyniak et al. [15] advanced this branch of the literature substantially. Their advection–diffusion algorithm emphasized modularity across one to three dimensions, support for common velocity sets, and improved complexity through more efficient encoding and collision building blocks. The authors also stressed that an LBM approximation for the advection–diffusion equation solves a modified equation instead of the exact continuum PDE, a point that remains central to any rigorous QLBM review. Classical consistency analysis therefore remains obligatory alongside algorithm design.

Xu et al. further improved the linearized collision treatment for advection–diffusion, proposing an ancilla-free or reduced-overhead formulation that better exploited quantum parallelism under a linear collision model [48]. Schalkers and Möller developed an efficient fail-safe quantum transport formulation that complements the LBM-based ADE route [47]. Independent one-dimensional quantum ADE algorithms also appear in the fluids literature [60]. Collectively, these works show that the advection–diffusion class has become a common proving ground for QLBM because it isolates tractable parts of the method while still preserving nontrivial transport structure.

3.2 From Linear Transport to Navier–Stokes-Oriented QLBM

A second branch of the literature attempts to extend QLBM beyond linear transport toward fluid flow proper. Budinski's streamfunction–vorticity formulation for the Navier–Stokes equations is a notable early milestone here [14]. Instead of tackling the primitive-variable incompressible system directly, the work used a reformulation that fits more naturally within an LBM timestep procedure. This illustrates a recurring pattern in QCFD. Progress often depends less on "solving Navier–Stokes on a quantum computer" in the usual textbook sense than on finding physically meaningful reformulations whose algebraic structure is more favorable.

Kumar and Frankel proposed a quantum unitary matrix representation of the LBM for low-Reynolds-number flow simulation [40]. Their formulation relied on singular-value decomposition (SVD) and careful state preparation to represent collision and streaming through products of unitary operations. The benchmark set included advection–diffusion, Poiseuille flow, Couette flow, and lid-driven cavity flow. From a CFD perspective, the main contribution lies in making gate-count and qubit-cost discussion explicit alongside reproduction of classical benchmark cases. Low-Reynolds-number benchmark agreement alone carries limited weight for viability at larger scales.

Zeng et al. introduced a hybrid quantum-classical LBM with a linearized non-equilibrium collision operator and modular circuit structure for practical flow simulation [49]. This line of work is important because it reflects a shift from purely conceptual quantum-fluid algorithms toward algorithms designed around current or near-term constraints. Hybridization acknowledges that different parts of the LBM update may belong on different hardware, instead of forcing the whole method to remain fully quantum. Complementary lines target nonlinear collisions, dissipative relaxation, realizability, and circuit complexity. Itani et al. formulate a quantum algorithm for lattice Boltzmann (QALB) update with a nonlinear collision term for incompressible flow [53]. Tiwari et al. analyze algorithmic requirements for a more realizable QLBM under hardware constraints [61]. Lăcătuş and Möller study surrogate quantum circuits for the lattice Boltzmann collision operator [62]. Khan et al. propose a deterministic realization of classical dissipative MRT relaxation on quantum computers, using a signed two-rail encoding and open-system amplitude-damping construction to avoid the success-probability loss associated with block-encoding the dissipative relaxation block [63]. Lee et al. propose a multiple-circuit decomposition to reduce quantum resources in QLBM workflows [51].

3.3 Dynamic Circuits and Multiple Time Steps

A recurring obstacle in QLBM has been the need to measure and reinitialize the state after each time step. This overhead can erase any plausible quantum benefit. Wawrzyniak et al. addressed this problem with a dynamic-circuit formulation in which the collision operator is implemented as a fully unitary process, enabling multiple time steps without full state reinitialization [50]. Lee et al. and Tiwari et al. pursue complementary routes toward resource-reduced and realizable multi-step QLBM implementations [51,61]. The dynamic-circuit work also reduced the dependence of ancilla overhead on the velocity set, which is significant because qubit costs tied directly to larger lattices would otherwise scale poorly.

In practical CFD, stable long-time marching defines feasibility as much as per-step accuracy. Quantum fluid solvers that stall after a handful of steps carry limited engineering meaning.

3.4 Toward Nonlinear and Turbulence-Relevant QLBM

Earlier nonlinear lattice-model and Carleman-lattice-Boltzmann constructions showed how multi-dimensional nonlinear updates and moderate-Reynolds-number fluid circuits can be expressed in quantum form [52–54,64]. A notable recent step toward nonlinear QLBM is the 2025 work by Wang et al. [16]. The study introduced a node-level ensemble description of a lattice-gas formulation, enabling a QLBM framework for nonlinear fluid dynamics. Reported demonstrations included vortex-pair merging and decaying turbulence, with simulations reaching up to 16.8 million computational grid points. This represents an important advance beyond earlier QLBM demonstrations that focused mainly on linear transport or more restricted flow settings. At the same time, industrial turbulence on quantum hardware remains out of reach. The contribution is therefore best interpreted as a more direct treatment of nonlinear structure within QLBM, without implying near-term industrial hardware advantage.

This work marks a promising broadening of the literature. For several years, much QLBM work could be viewed as concentrated on quantum-advection-diffusion-style benchmarks. The Wang et al. result indicates that nonlinear fluid dynamics is now being confronted more directly, even if the path to engineering LES or DNS remains long [16]. Recent work also reports QLBM demonstrations on real quantum devices, including linear-acoustics-oriented examples [65], and nontrivial incompressible-flow benchmarks with a QLBM algorithm [55].

3.5 What Would It Mean for QLBM to Become Relevant for DNS, LES, and Hybrid Turbulence Workflows?

Large-eddy simulation (LES) filters the Navier–Stokes equations and models unresolved stresses through a subgrid-scale (SGS) closure. In wall-modeled LES, the outer-flow discretization is additionally coupled to a near-wall model. Classical LES commonly relies on eddy-viscosity and related closures, including Smagorinsky-type models [66] and dynamic formulations [67,68]. Homogeneous turbulence simulations also require carefully designed forcing to maintain statistical stationarity [69]. In lattice Boltzmann formulations, body forces must be introduced in a way that preserves consistency with the discrete lattice [70]. Foundational reviews of LBM for fluids [71,72] document the classical capabilities and complexity that QLBM development must address to approach engineering-relevant turbulence regimes. Classical LBM has a long history in turbulence simulation and high-performance implementation, including early discussions of lattice-Boltzmann computing challenges, massively parallel turbulent-channel simulations, direct and large-eddy simulations of turbulent flow, and decaying homogeneous isotropic turbulence benchmarks [73–76]. For LES, the subgrid-scale closure should be introduced consistently at the kinetic or mesoscopic level, which has motivated dedicated SGS formulations for lattice Boltzmann methods [77].

The focus on LES is intentional because LBM–LES and wall-modeled LBM are already established parts of classical mesoscopic turbulence simulation and are directly relevant to aeroacoustic source prediction. DNS provides a stricter validation target for future QLBM, since it would require fully resolved nonlinear time marching, controlled dissipation and dispersion, and recovery of long-time turbulence statistics. Hybrid Reynolds-averaged Navier–Stokes–large-eddy simulation (RANS–LES) approaches, including DES, improved delayed detached-eddy simulation (IDDES), unsteady Reynolds-averaged Navier–Stokes–computational aeroacoustics (URANS–CAA) chains, and wall-modeled large-eddy simulation (WMLES)-type workflows, are also relevant from an industrial perspective; in such settings, QLBM would more plausibly enter as a targeted transport, source-region, linearized-acoustic, or design-loop component while turbulence modeling, wall treatment, geometry handling, and source extraction remain coupled workflow elements.

For QLBM to become relevant to DNS, LES, or hybrid RANS–LES workflows, reproducing homogeneous decaying turbulence on a quantum circuit would be insufficient on its own. That would test only part of the problem. The harder requirement is to handle heterogeneous flow settings with walls, pressure gradients, moving bodies, and long-time integration that produces statistically meaningful outputs. Homogeneous-turbulence benchmarks are still useful because they test nonlinearity and resolution scaling without the added complexity of geometry. They play a similar role in classical algorithm development [76]. Recent LBM-LES work on forced homogeneous isotropic turbulence (FHIT) asks whether kinetic-level coarse-graining keeps the solver in a hydrodynamic regime compatible with conventional subgrid-stress modeling. That assessment uses a turbulent Knudsen number diagnostic together with spectra and higher-order statistics [78]. In parallel, physics-constrained neural closures for LBM-LES, trained on filtered DNS fields, show how classical methods already combine mesoscopic numerics with data-driven SGS models and deployment-oriented coupling [79]. These studies set a demanding classical benchmark that any quantum or hybrid QLBM accelerator must clear before it can be considered useful for turbulence-relevant applications. Mesoscopic LBM has also been applied to more complex interfacial turbulence, including immiscible Rayleigh–Taylor turbulence, which broadens the classical turbulence baseline beyond periodic single-phase tests [80].

From a QLBM perspective, an LES-relevant research program would eventually need three elements. First, it would need stable long-time marching with measurement strategies that can recover spectra and second-order statistics. Second, it would need boundary models that go beyond periodic boxes. Third, it would need either explicit subgrid modeling within the lattice formalism or a defensible hybrid split in which quantum kernels accelerate only resolved-scale transport, while closures remain classical. This division would be similar to the way industrial LES already separates numerical solution from physical modeling.

Until these elements are available, QLBM is better viewed as a possible mesoscopic accelerator within selected parts of a workflow, instead of a direct replacement for LES. This position is also consistent with classical LBM practice. Wall-modeled LBM LES is now a developed classical research direction, with explicit wall models, high-Reynolds-number channel-flow studies, and systematic comparisons of collision schemes, SGS models, and wall functions [81–83]. Recent LBM LES work also couples near-wall modeling with synthetic-turbulence generation and physics-informed data-driven wall models, setting a higher classical baseline than minimal toy LBM simulations [84,85]. Dynamic subgrid modeling on the lattice [86] and entropic-LBM turbulence statistics [87] show that classical LBM stacks are already highly developed. Future QLBM benchmarks should therefore be tested against both minimal toy LBM baselines and this class of optimized classical workflow. Table 2 contrasts classical LBM and LES baselines with plausible near-term quantum target subproblems.

Table 2: Classical LBM and LES baselines vs. plausible near-term quantum targets for wall-modeled large-eddy simulation (WMLES), homogeneous isotropic turbulence (HIT), forced homogeneous isotropic turbulence (FHIT), subgrid-scale (SGS) modeling, boundary conditions (BCs), finite element method (FEM), boundary element method (BEM), linearized Navier-Stokes equations (LNSE) acoustic blocks, physics-informed neural network (PINN) wall models, and quantum linear systems algorithm (QLSA) routes. Realism indicates how credible end-to-end deployment is on present or announced hardware, using an ordinal scale rather than a calendar forecast.

Classical Stack	Current Capability	Quantum Target Subproblem	Realism	Main Bottleneck
LBM-LES, WMLES, and closures	GPU/HPC mesoscopic solvers [88,89]; FHIT validation and neural LBM-LES closures [78,79]; PINN wall models [85]	Hybrid: linearized collision and stream substeps; outer-loop surrogates	Mid–long	Nonlinearity, readout, industrial BCs
LES forcing and SGS on lattices	Smagorinsky and dynamic SGS [66,67]; stationary HIT forcing [69]; consistent LBM forcing [70]	Occasional linear solves in coupled blocks, rather than replacement of classical SGS	Long	Physics modeling vs. algorithmic overhead
Foundational LBM for complex flows	Theory and practice at engineering complexity [71,72]	QLBM kernels, hybrid circuits, proof-of-concept benchmarks	Near–mid	Unitary embedding, encoding, measurement
Pressure, Helmholtz, and linear acoustics	Sparse FEM/BEM, coupled LNSE–Helmholtz in CAA [22]	VQLS and QLSA on sparse blocks; frequency-domain solves	Near–mid	Preconditioning, state preparation

3.6 Boundary Conditions, Bounce-Back, and Complete Formulations

In classical LBM, boundary treatment is often where elegant theory meets engineering reality. Quantum formulations face the same tension. Liu et al. recently proposed a complete formulation based on linear equilibrium distribution functions, incorporating bounce-back boundary conditions directly into the collision matrix and representing streaming through conditional unitary shift operations [17]. Schalkers and Möller have also emphasized that data encoding and momentum-exchange boundary forcing are central to the realism of quantum Boltzmann methods [90,91]. Recent boundary-focused QLBM work further develops coherent implementations of bounce-back and specular-reflection-type boundary conditions, reinforcing boundary treatment as a core algorithmic issue rather than a post-processing detail [92]. These developments matter because they treat boundary conditions and observables as integral parts of the quantum formulation.

For an engineering-facing review, such developments matter. A quantum algorithm that reproduces only periodic or highly idealized domains may be interesting, yet it leaves open the wall-bounded and installed-flow settings relevant to fans, propellers, ducts, liners, and rotating machinery. Progress on boundary representation therefore benefits from more attention than is sometimes given in purely algorithmic reviews. Complementary benchmark-oriented work has established a reproducible D3Q19 MRT-LBM

Poiseuille-flow test with body forcing, bounce-back walls, analytical verification, and an operator-level audit for future quantum and hybrid implementations [93].

3.7 Software Ecosystems and Reproducibility

Maturing scientific fields eventually develop software infrastructure, and QLBM is beginning to do so. Georgescu et al. introduced a dedicated software framework for QLBM, designed to generate, simulate, and analyze quantum circuits for two- and three-dimensional CFD problems [58]. Shinde et al. reported an Intel Quantum software development kit (SDK) implementation of QLBM that illustrates how classical software-engineering practice can be transferred to quantum circuit development [57]. Bharadwaj's QFlowS likewise contributes tooling for quantum fluid-circuit construction and experimentation [56]. Such frameworks primarily support reproducibility and scaling studies beyond isolated demonstrations that remain largely proof-of-concept. Physical usefulness still rests on validation against classical baselines.

The most mature entries in the table are therefore not simply the most recent ones, but those that combine a clear physical target with benchmark evidence and explicit resource reporting; conversely, papers that introduce important formulations but leave qubit, gate-depth, measurement, or classical-baseline costs unspecified should be read as methodological advances rather than engineering-ready demonstrations.

Table 3: Critical comparison of representative QLBM and QLBM-tooling literature, including singular-value decomposition (SVD)-based unitary-factor approaches where relevant. The table emphasizes the physical target, algorithmic distinction, reported evidence or resource information, and remaining validation need for engineering CFD/CAA.

Reference	Physical Target	Algorithmic Distinction	Reported Evidence/Resource Status	Remaining CFD/CAA Limitation
Budinski [13], 2021	Advection–diffusion via LBM	Introduced an early collision–streaming QLBM template with initialization, collision, propagation, and measurement.	Demonstrated the algorithmic structure for linear transport; full CFD-scale qubit, gate-depth, and measurement budgets were outside the main focus.	Leaves nonlinear collision, acoustic-source generation, complex boundaries, and CAA observables outside the present validation scope.
Budinski [14], 2022	Incompressible flow, streamfunction–vorticity	Extended QLBM concepts toward Navier–Stokes-type flow using a reformulation compatible with LBM time stepping.	Provided a route beyond scalar transport, but the formulation remains tied to reformulated variables rather than a complete primitive-variable engineering solver.	Needs stronger connection to pressure/velocity fields, wall-bounded flow, and acoustic source quantities.
Wawrzyniak et al. [15], 2025	Advection–diffusion QLBM	Developed a modular multidimensional ADE formulation with improved encoding and support for common velocity sets.	Reports improved algorithmic construction for linear ADE settings; resource discussion is mainly algorithmic, while CFD-scale qubit, gate-depth, and measurement budgets remain only partially specified.	Modified-equation consistency, nonlinear flow extension, and acoustic-observable recovery remain open for CFD/CAA use.

(Continued)

Table 3 (continued)

Reference	Physical Target	Algorithmic Distinction	Reported Evidence/Resource Status	Remaining CFD/CAA Limitation
Xu et al. [48], 2025	Linear-collision ADE	Reduced ancilla or collision overhead by exploiting the structure of a linearized collision model.	Useful resource improvement for a restricted linear setting; no demonstration of full nonlinear LBM or aeroacoustic prediction.	Extension to nonlinear equilibrium, forcing, boundary conditions, and pressure-fluctuation observables remains necessary.
Kumar and Frankel [40], 2025	Unitary LBM flow benchmarks	Used SVD-based unitary factors for ADE, Poiseuille, Couette, and lid-driven-cavity benchmarks.	Includes qubit and gate-cost discussion alongside comparison with classical benchmark behavior.	Benchmark agreement at low Reynolds number does not yet establish scalability against optimized classical LBM or CAA workflows.
Zeng et al. [49], 2025	Hybrid practical-flow QLBM	Introduced a modular hybrid formulation with a linearized non-equilibrium collision operator.	Important near-term direction because it avoids forcing all LBM operations into a fully quantum pipeline.	Linearized collision, wall treatment, nonlinear physics, and CAA-grade boundary conditions require further validation.
Wawrzyniak et al. [50], 2025	Multi-step QLBM	Used dynamic circuits to reduce repeated measurement and reinitialization across time steps.	Targets a major resource bottleneck in time-marched QLBM by enabling multiple steps before full readout.	Long-time stability, noise accumulation, spectra, and field-statistics extraction remain to be demonstrated for engineering problems.
Wang et al. [16], 2025	Nonlinear flow and decaying turbulence	Advanced QLBM beyond linear transport using an ensemble or lattice-gas construction for nonlinear dynamics.	Reported substantially larger nonlinear-flow demonstrations than earlier linear-transport studies.	Industrial turbulence, wall-bounded LES, moving geometry, acoustic source spectra, and hardware-level resource accounting remain unresolved.
Liu et al. [17], 2026	QLBM with boundary treatment	Built bounce-back-type boundary treatment into the collision-matrix formulation and used conditional unitary streaming.	Significant because boundary handling is treated as part of the algorithm rather than as an afterthought.	Generality beyond linear equilibrium, simplified walls, and periodic or idealized settings still needs to be established.
Georgescu et al. [58], 2025	QLBM software framework	Provided tools for generating, simulating, and analyzing QLBM circuits in two- and three-dimensional settings.	Improves reproducibility and enables circuit-level scaling studies.	Software maturity alone does not establish physical validity; benchmark comparison with classical CFD/CAA remains essential.
Bharadwaj [56], 2024	Quantum-fluid circuit tooling	Provided infrastructure for constructing and testing quantum fluid-flow circuits.	Useful for exploratory circuit development and workflow standardization.	A gap remains between circuit construction and validated CFD/CAA prediction with physical observables.

3.8 *Critical Synthesis across QLBM Streams*

The literature reviewed above shows progress along several different axes, and these axes require separate assessment. Linear ADE and scalar-transport QLBM papers are the most mature algorithmically because they isolate encoding, streaming, and collision with relatively clean consistency checks. They are therefore useful benchmark platforms, yet readiness for nonlinear flow or acoustic-source prediction remains to be demonstrated separately. NS-oriented and nonlinear/turbulence-oriented QLBM papers are physically more ambitious, yet their additional expressiveness is obtained through streamfunction–vorticity reformulations, linearized or hybrid collision models, Carleman lifting, ensemble constructions, or lattice-gas analogues, all of which introduce their own overhead or regime restrictions. Dynamic-circuit and unitary-factorization studies attack an important time-marching bottleneck, while stable long-time statistics, norm control, and economical readout remain open requirements. Boundary-focused work is particularly important for engineering CFD because periodic domains are rarely the final target, yet existing demonstrations still fall short of the moving, curved, impedance, and installed-flow boundaries that dominate practical CAA.

Table 4 summarizes the main QLBM-related literature streams by landmark contribution, relative strength, and remaining CFD/CAA limitation.

This comparison suggests a different prioritization from a purely chronological literature survey. For near-term engineering value, the most promising QLBM-related directions combine modest physical scope with explicit resource accounting, boundary handling, and observable-level validation. Weakly compressible linear acoustics, scalar transport with controlled modified-equation error, and hybrid Helmholtz or linearized Navier–Stokes (LNSE) blocks have clearer output targets than a full turbulent-flow field. Conversely, QLBM claims aimed at LES, aeroacoustic source generation, or rotating machinery need substantially stronger evidence: stable multi-step evolution, credible boundary models, comparison against optimized GPU/HPC LBM, and readout strategies for spectra, correlations, forces, or pressure signals. This is why the roadmap later in the paper treats QLBM as a selective workflow component rather than a near-term replacement for established CFD/CAA solvers. The illustrative QLBM uplift in Section 10 is presented for the same reason: as a benchmark architecture and reporting template for future resource analysis, rather than as a completed quantum implementation or quantum-advantage demonstration.

Table 4: Critical comparison of major QLBM-related literature streams. The table separates landmark value from remaining limitations so that algorithmic progress is distinguished from engineering readiness.

Stream	Landmark Contribution	Relative Strength	Main Limitation for CFD/CAA
Linear ADE and scalar-transport QLBM [13,15,47,48]	Established tractable collision–streaming templates and improved encoding or collision overhead for linear transport.	One of the most mature current platforms for consistency checks, circuit construction, and reproducible small-grid benchmarks.	Linear scalar physics leaves nonlinear equilibrium, acoustic-source generation, wall-bounded flow, and full-field readout at engineering scale outside the present validation scope.
NS-oriented QLBM [14,17,40,49]	Moved the discussion from scalar transport toward flow variables, incompressible formulations, linearized non-equilibrium collision, and boundary-aware updates.	Most relevant bridge from QLBM methodology to recognizable fluid-mechanics benchmarks.	Often relies on reformulated variables, linearized collision physics, simplified boundaries, or limited validation regimes; primitive-variable and CAA observables remain underdeveloped.

(Continued)

Table 4 (continued)

Stream	Landmark Contribution	Relative Strength	Main Limitation for CFD/CAA
Dynamic, unitary, and multi-step formulations [40,50,51,61]	Addressed unitary embedding and repeated time marching, including SVD/unitary-factor approaches and dynamic circuits.	Targets a genuine QLBM bottleneck: repeated measurement and re-initialization across time steps.	Long-time stability, norm control, gate depth, noise accumulation, and extraction of spectra or statistics remain insufficiently demonstrated.
Nonlinear and turbulence-oriented QLBM [16,52–55]	Attempts to include nonlinear collision or turbulent-flow behavior through Carleman, lattice-gas, ensemble, or related constructions.	Physically more ambitious than linear transport and therefore important for the long-term relevance of QLBM.	System-size growth, truncation error, closure modeling, wall-bounded turbulence, moving geometry, and LES-level validation remain open.
Boundary-focused QLBM and software infrastructure	Boundary-focused studies address data encoding, momentum exchange, bounce-back treatment, and conditional streaming [17,90,91]. Software frameworks support reproducible circuit generation and implementation studies [56–58].	Important for moving beyond ideal periodic boxes and isolated proof-of-concept circuits.	Complex geometry, moving walls, impedance or absorbing acoustic boundaries, and validation against mature classical LBM stacks remain largely unresolved.
Hybrid QCFD linear-solver interfaces	Quantum linear-system algorithms provide the foundation for sparse linear solves [29,45]. CFD-oriented studies apply or benchmark these methods in finite-volume, pressure-Poisson, and related solver blocks [30–33].	Likely the clearest near-term interface with decomposed engineering workflows.	Addresses subproblems within CFD/CAA workflows rather than a full QLBM solver; speedup depends on preconditioning, data loading, output compression, and fair comparison with optimized classical linear solvers.

4 Cross-Cutting Technical Challenges in QLBM

4.1 Nonlinearity Handling

The central difficulty in fluid dynamics is nonlinearity. Several strategies appear in the literature, including linearized equilibria, truncated Carleman linearization, streamfunction–vorticity reformulations, ensemble or lattice-gas transforms, and hybrid classical–quantum splitting. Each strategy buys tractability at a price. Linearized equilibria may restrict the physical regime. Carleman methods increase system dimension. Hybrid splitting reduces the amount of genuinely quantum computation. Ensemble methods introduce alternative representational overhead. A balanced review treats these strategies as partial solutions instead of universal remedies.

4.2 State Preparation and Measurement

The promise of amplitude encoding is that a large state can be represented compactly in qubits. State preparation and readout are nonetheless central bottlenecks. Preparing physically meaningful distributions may require structured loading assumptions or quantum random access memory (qRAM) access, and useful output usually arrives only through statistical measurement routines [94–96]. QLBM intensifies this issue because CFD users rarely want a single scalar answer. They usually want fields, spectra, forces, moments, or statistics over many time steps. Classical shadow protocols provide one possible route for reducing measurement overhead when many quantities must be estimated [97]. The more field information must be extracted, the harder it is to preserve any putative speedup.

4.3 Comparison with Optimized Classical LBM

Another underappreciated issue is the baseline for comparison. Graphics processing unit (GPU) implementations can achieve strong LBM performance through optimized memory-access strategies [88]. Mixed-precision implementations can further reduce memory requirements and improve performance while retaining suitable accuracy [89]. These results motivate using optimized GPU and high-performance computing (HPC) LBM implementations, rather than unoptimized serial codes, as baselines for assessing QLBM advantage claims. Classical LBM also has mature high-performance and complex-geometry applications. Exascale-oriented studies and large-scale simulations involving biological or built porous structures illustrate the strength of modern classical implementations [98–101]. Non-ideal and multiphase capabilities are further demonstrated by multirange pseudopotential and high-density-ratio phase-separation formulations [102,103]. Application-specific multiphysics LBM studies, including phase-change-enhanced hydrogen-storage modelling, further show that the classical LBM comparator is broader than single-phase transport [104]. Classical LBM can also be enhanced by data-driven wall models, synthetic turbulence generators, and other accelerators [84,85]. Assessing QLBM's future relevance requires comparison with modern classical LBM, including optimized and data-augmented stacks, instead of minimal or unoptimized classical baselines alone. Fig. 6 summarizes how representative QLBM and hybrid QCFD routes treat these cross-cutting bottlenecks from an engineering CFD perspective.

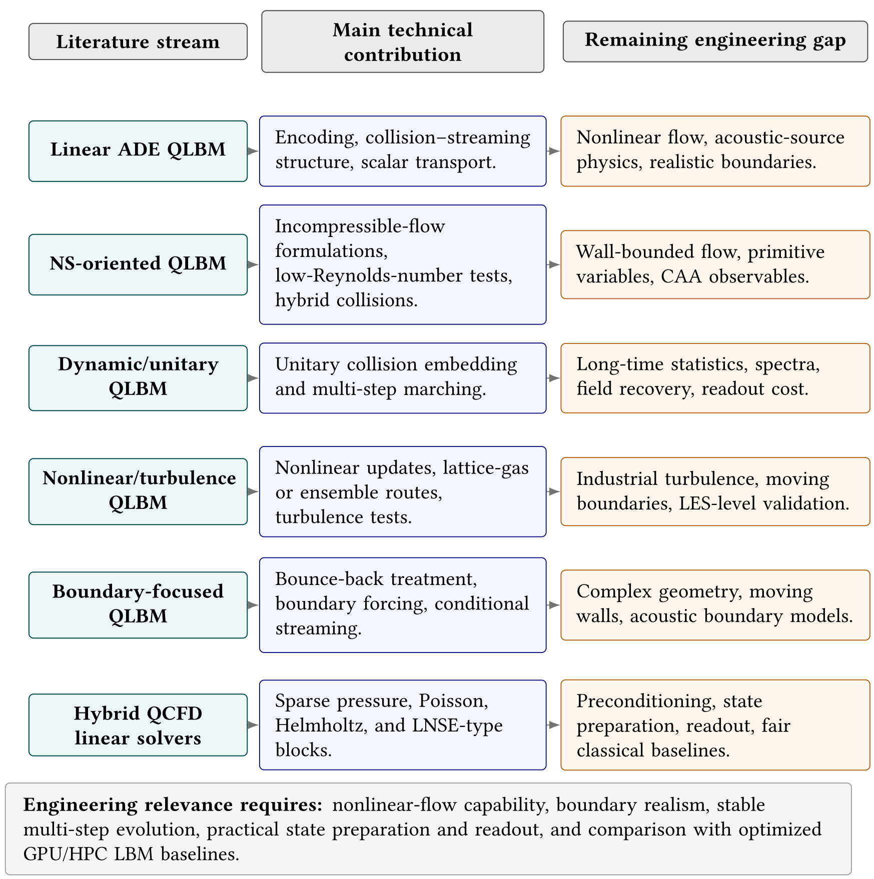

Figure 6: Evidence-linked bottleneck map for QLBM from an engineering CFD perspective. The literature streams follow the hybrid QCFD background and QLBM thematic branches in Sections 2 and 3. Early and modular linear

(Continued)

Figure 6: (continued) ADE QLBM formulations are represented by [13,15,47], while reduced-overhead and independent ADE developments are represented by [48,60]. NS-oriented QLBM includes streamfunction–vorticity, unitary, and hybrid collision formulations [14,40,49]; related realizability and surrogate-collision studies are represented by [61,62]. Dynamic and unitary QLBM work addresses unitary factorization, repeated time marching, and resource reduction [40,50,51,61]. Nonlinear and turbulence-oriented developments include Carleman and nonlinear collision formulations [52–54,64], while ensemble and nontrivial-flow studies are represented by [16,55]. A real-device QLBM demonstration, including a linear-acoustics-oriented application, is represented by [65]. Boundary-focused work addresses bounce-back, data encoding, and momentum exchange [17,90,91]. Hybrid QCFD linear-solver interfaces include finite-volume and hybrid flow-solver studies [30,31], together with pressure-Poisson and broader hybrid CFD workflow studies [32–34]. The figure summarizes the main technical contributions and remaining engineering gaps, emphasizing that practical CFD/CAA use still requires stronger treatment of nonlinear flow, boundary realism, stable multi-step evolution, measurement/readout, and comparison with optimized classical LBM baselines.

5 Classical LBM as a Bridge to QLBM for Engineering Use

Classical LBM practice is the natural reference when judging QLBM proposals for aeroacoustic and propulsion-related transport. Wall-resolved and wall-modeled LES on the lattice, synthetic inflow for WMLES, GPU-oriented implementations, and physics-informed near-wall modeling already define the performance bar for mesoscopic solvers [78,79,84,85]. The following subsection states the shared mathematical skeleton that QLBM work typically assumes before discussing quantum encodings.

This bridge section defines the standard against which QLBM claims should be judged, rather than simply restating the familiar LBM update. A quantum formulation that reproduces only the collision–streaming skeleton but omits forcing, boundaries, turbulence closure, readout, or comparison with optimized classical LBM has demonstrated algorithmic structure without yet establishing engineering CFD capability.

5.1 Mathematical Backbone of Classical LBM and QLBM

The following equations provide a compact anchor for the rest of the review. Concrete lattice sets, collision models, and quantum encodings vary across papers, so the notation is intentionally schematic.

For incompressible flow, the classical macroscopic system is

$$\nabla \cdot \mathbf{u} = 0, \tag{1}$$

$$\frac{\partial \mathbf{u}}{\partial t} + (\mathbf{u} \cdot \nabla)\mathbf{u} = -\frac{1}{\rho}\nabla p + \nu \nabla^2 \mathbf{u} + \mathbf{f}. \tag{2}$$

For scalar advection–diffusion benchmarks, a common companion is

$$\frac{\partial \phi}{\partial t} + \mathbf{u} \cdot \nabla \phi = D\nabla^2 \phi + S. \tag{3}$$

Classical mesoscopic lattice methods trace back to lattice-gas and lattice-Boltzmann formulations [105]. The Bhatnagar–Gross–Krook (BGK) relaxation model [106] provided one of the earliest compact collision models, while lattice BGK (LBGK) and incompressible LBGK analyses clarified how Navier–Stokes recovery, dispersion, dissipation, isotropy, Galilean invariance, and stability depend on the collision model and relaxation parameters [107–109]. In compact form,

$$f_i^*(\mathbf{x}, t) = \mathcal{C}_i[\mathbf{f}(\mathbf{x}, t)], \tag{4}$$

$$f_i(\mathbf{x} + \mathbf{c}_i \Delta t, t + \Delta t) = f_i^*(\mathbf{x}, t). \tag{5}$$

Here $\mathcal{C}$ denotes the chosen collision model. In simple BGK LBM it is a single-relaxation-time relaxation toward equilibrium, while in the benchmark developed later in this paper it is the D3Q19 MRT collision written in moment space. Macroscopic density and momentum are recovered as

$$\rho = \sum_i f_i, \qquad \rho\mathbf{u} = \sum_i \mathbf{c}_i f_i.$$

For weakly compressible acoustic LBM, pressure fluctuations are obtained from the lattice equation of state.

QLBM work typically encodes mesoscopic degrees of freedom in a quantum state and seeks streaming and collision updates compatible with quantum operations. A schematic encoding is

$$|\psi(t)\rangle = \sum_{\mathbf{x},i} \alpha_{\mathbf{x},i}(t)\,|\mathbf{x}\rangle \otimes |i\rangle, \tag{6}$$

with an abstract step (concrete unitaries, ancillas, and hybrid steps differ by paper) such as

$$|\psi(t+\Delta t)\rangle \approx U_{\text{stream}}\,U_{\text{coll}}\,|\psi(t)\rangle, \tag{7}$$

The recovered macroscopic observables can be written schematically as

$$m_k(\mathbf{x},t) = \langle\psi(t)|\hat{M}_k(\mathbf{x})|\psi(t)\rangle, \tag{8}$$

$$|\psi(t+\Delta t)\rangle \approx U_{\text{stream}}\,U_{\text{coll}}[m_k]\;|\psi(t)\rangle. \tag{9}$$

Here $\hat{M}_k$ denotes an observable associated with the macroscopic quantities of interest (e.g., density, momentum, or other moments), while the bracketed dependence indicates that in many practical or hybrid formulations the collision step can depend on classically reconstructed moments instead of a closed-form unitary realization of the full nonlinear update. These two relations make explicit why readout cost and hybridization recur throughout the QLBM literature. In this sense, the practical distinction between QLBM proposals often lies less in the continuum equations targeted than in the choice of encoding, the realization of non-unitary collision physics, and the observables that must be measured at each step. In this schematic, U_{stream} realizes lattice advection as a permutation-like map on encoded indices, while U_{coll} denotes a unitary embedding, approximation, or hybrid implementation of the generally non-unitary classical collision. This overall picture is why the literature emphasizes linearized collisions, ancilla constructions, and dynamic or decomposed circuits instead of a single closed-form unitary for full BGK/MRT physics.

Boundary treatment remains central in LBM practice. Velocity and pressure boundaries are often based on the Zou–He construction, while curved or moving boundaries can be handled through interpolated bounce-back and momentum-transfer methods [110–112]. No-slip walls are often imposed with bounce-back rules that relate populations on incoming and outgoing lattice links at wall nodes. Section 6 treats boundary realism as a separate evaluation axis because quantum formulations must encode these rules compatibly with streaming and measurement.

Classical LBM evolves distribution functions over a discrete set of lattice velocities. Each timestep combines a local collision operation with streaming to neighboring nodes. This structure maps naturally to population-level linear algebra, permutation-like advection, and moment-based physics, which are all features commonly used in QLBM constructions. Important limitations remain, including non-unitary collisions, boundary treatment, nonlinear equilibria, and the cost of reading out full fields from encoded quantum states. Fig. 7 decomposes a QLBM-style timestep into encoding, collision, streaming, measurement, and time marching. The dashed callouts highlight the main technical pressure points that recur across the literature.

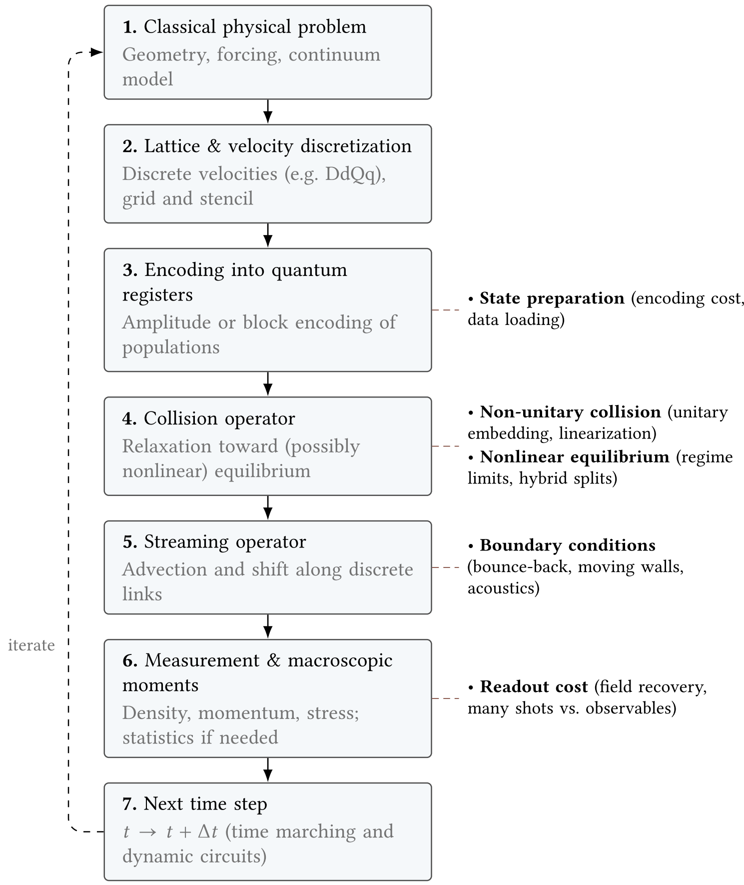

Figure 7: Schematic anatomy of a quantum lattice Boltzmann workflow, starting from the classical problem statement and moving through discretization, quantum encoding, collision and streaming, measurement of macroscopic moments, and time marching. Dashed lines indicate the main pressure points discussed throughout the QLBM literature, including state preparation during encoding, non-unitary and nonlinear collision physics, boundary treatment during streaming, and readout when recovering fields or statistics.

5.2 Critical Implications for QLBM Claims

The comparison with classical LBM leads to three practical filters for evaluating future QLBM proposals. First, a physical-equivalence filter is needed: the quantum update should specify which continuum or lattice equation it approximates, whether the collision model is BGK, MRT, linearized, or lifted, and whether the recovered macroscopic variables have the same meaning as in the classical solver. This is especially important in acoustics, where small density and pressure fluctuations, dispersion, and dissipation errors can matter even when bulk flow variables appear accurate. Second, a workflow-equivalence filter is needed: the proposed quantum block should identify whether it replaces a transport kernel, a collision step, a source-region model, a linear propagation solve, or a design-loop calculation. Without that separation, end-to-end resource claims become difficult to interpret because state preparation and readout can dominate the cost of apparently compact amplitude encodings. Third, a performance-equivalence filter is needed: the baseline should be a modern GPU/HPC or otherwise optimized LBM/CAA implementation, rather than serial pedagogical code. These filters convert the classical–quantum connection from a loose analogy into an explicit validation checklist.

For the present aeroacoustic focus, the most demanding outputs include pressure spectra, directivity, phase, source strength, wall-pressure correlations, and receiver-side sound metrics, in addition to density or velocity snapshots. Without controlled sampling cost for such observables, a QLBM method will remain difficult to use even if its internal collision–streaming circuit is elegant. Conversely, a limited QLBM or hybrid quantum block can still be valuable if it is inserted at a well-defined place in the CAA chain and reports the same acoustic quantities used by classical workflows. The benchmark and illustrative uplift developed later in the paper are framed with this narrower standard in mind.

6 How to Evaluate Quantum CFD from a Fluids Perspective

Many discussions of QCFD naturally emphasize quantum-algorithmic structure, hardware scaling, and asymptotic complexity. These issues are essential, yet they remain insufficient from the viewpoint of fluid simulation. For CFD practitioners, a useful evaluation framework must also ask what equations are being solved, how nonlinearities are treated, which boundary conditions are represented, what physical regime is addressed, and what classical baseline is used for comparison.

This review adopts the following criteria.

1. **Physical scope.** Does the method address advection–diffusion, incompressible flow, compressible flow, weakly compressible transport, turbulence, or acoustics?
2. **Algorithmic realism.** Are nonlinearity, state preparation, and measurement explicitly accounted for, or are they hidden behind idealized assumptions?
3. **Boundary-condition realism.** Can the method accommodate solid walls, moving walls, bounce-back rules, immersed geometries, or acoustic boundary models in a credible way?
4. **Hardware relevance.** Is the algorithm intended for noisy intermediate-scale quantum (NISQ) hardware, for a hybrid classical–quantum setting, or for a more distant fault-tolerant era?
5. **Engineering comparability.** Is the quantum method compared against optimized classical CFD/LBM, or only against simplified classical baselines?

These criteria help separate mathematically interesting quantum reformulations from methods that are likely to become useful for CFD practice. A method may be elegant from the standpoint of quantum algorithm design while still being restricted by its physical regime, boundary treatment, measurement cost, state-preparation assumptions, or comparison with classical solvers.

7 Aeroacoustics and Rotating Machinery: Engineering CAA Context

This section treats aeroacoustics and rotating machinery as the target application class for mapping quantum and hybrid methods onto established CAA practice, including decomposed chains from unsteady flow through sources, propagation, and design metrics. Classical CAA is rooted in acoustic-analogy theory, from Lighthill's formulation for flow-generated sound to the Ffowcs Williams–Hawkings (FW–H) extension for moving solid surfaces [20,21]. Modern reviews emphasize the separation between unsteady flow simulation, source extraction, acoustic propagation, and receiver metrics [23,113].

Industrial CAA already employs such decomposed chains (unsteady flow → sources → acoustics/propagation → metrics → design loops). That structure yields clear interfaces at which hybrid acceleration can be discussed, and it matches textbook and industrial descriptions of fan, propeller, and installed-noise practice [18,19,22].

The acoustic relevance of LBM is physical as well as algorithmic. Weakly compressible LBM can propagate sound waves and has developed into a mature tool for computational aeroacoustics and direct noise computation [114–117]. LBM has also been used for acoustic source identification, acoustic control, duct damping, and acoustic manipulation, which supports its role as a classical comparator for future

QLBM acoustic benchmarks [118–121]. Classical LBM recovers density and momentum from velocity-distribution moments, so pressure fluctuations are connected to density fluctuations through the lattice equation of state, while velocity, stress, and wall-pressure information can be extracted from hydrodynamic and non-equilibrium moments.

This classical LBM–acoustics foundation makes the QLBM question more precise. QLBM becomes acoustically relevant only when the quantum or hybrid formulation preserves the same source-bearing quantities that classical LBM uses for acoustics. These quantities include weak pressure and velocity fluctuations, non-equilibrium stress information, vorticity, wall-pressure signals, and long-time spectra. A QLBM proposal is acoustically meaningful when it can preserve and recover these observables with credible boundary treatment, measurement strategy, and comparison against classical LBM–CAA baselines. Fig. 8 summarizes this chain and turns it into evaluation criteria for QLBM and hybrid quantum–classical acoustics.

This mapping also clarifies why the relevant classical comparator is the existing LBM–CAA and linear-acoustics toolchain against which any QLBM or hybrid quantum contribution must be judged.

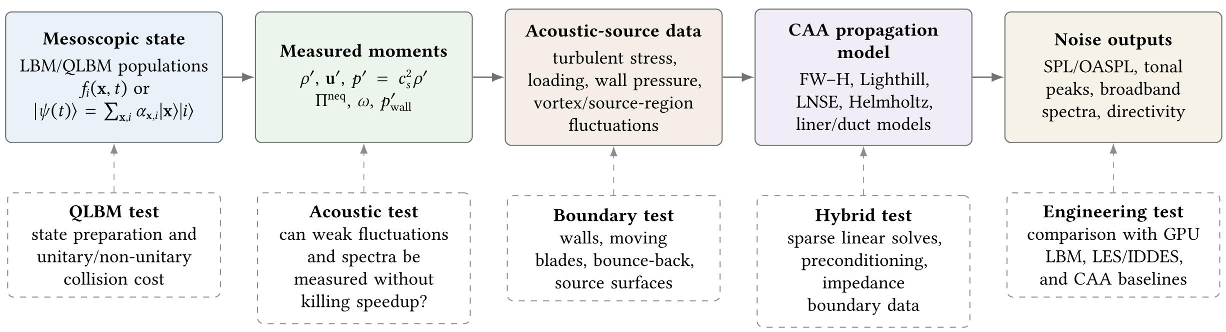

Figure 8: Physics map connecting LBM/QLBM variables to aeroacoustic observables. Mesoscopic populations or quantum-encoded populations must be converted into weak pressure/velocity fluctuations, non-equilibrium stresses, vorticity, and wall-pressure data before they become useful for acoustic-source descriptions. Propagation and radiation can then be handled by classical or hybrid CAA models such as the Ffowcs Williams–Hawkings (FW–H) analogy, Lighthill-type analogies, LNSE, Helmholtz, or liner/duct formulations. The noise outputs include sound pressure level (SPL), overall sound pressure level (OASPL), tonal peaks, broadband spectra, and directivity. The lower row lists the corresponding tests that any QLBM or hybrid quantum proposal must pass before it can be considered relevant to engineering aeroacoustics, including comparison with GPU LBM, LES/IDDES, and CAA baselines.

7.1 Classical LBM and Linear-CAA Baselines as Comparators

Claims about QLBM or hybrid quantum transport are most fairly assessed against the same classical LBM stacks used in turbulence and near-wall aeroacoustic-oriented LBM work. For aeroacoustic applications, LBM has been compared directly with high-order Navier–Stokes and finite-volume methods in terms of dispersion, dissipation, computational cost, and time to solution, which makes classical LBM a demanding comparator for future QLBM or hybrid quantum contributions [122–124]. Practical LBM CAA also depends on stabilization, regularization, grid refinement, and mesh coupling, because small pressure errors can contaminate acoustic predictions [125–129]. Multiblock, block-structured, non-uniform, and octree LBM meshes are especially relevant for engineering CAA because resolution is usually concentrated near walls, shear layers, source regions, and propagation paths rather than distributed uniformly across the full domain [130,131]. For QLBM, this adds a further challenge beyond uniform-lattice collision and streaming: block-interface coupling, prolongation/restriction, interpolation error, load balancing, and acoustic errors introduced at refinement interfaces must eventually be addressed.

Open-domain LBM aeroacoustics additionally requires careful boundary treatment, including non-reflecting boundary conditions, perfectly matched layer (PML) formulations, outflow treatments, and absorbing-layer analyses [132–135]. These stacks include wall-modeled LES with synthetic inflow, GPU-resolved regimes, forced-homogeneous diagnostics for subgrid modeling, and physics-informed or neural closures coupled to the lattice [78,79,84,85]. For propagation in liners and ducts, coupled linearized LNSE and Helmholtz formulations with viscothermal losses define a credible linear-algebraic subproblem class [22]. That setting is a useful comparator for hybrid quantum linear solvers because it isolates sparse structure without requiring full nonlinear turbulent CFD on a quantum processor. Fig. 9 sketches the decomposed CAA chain and highlights three hybrid insertion targets used repeatedly below.

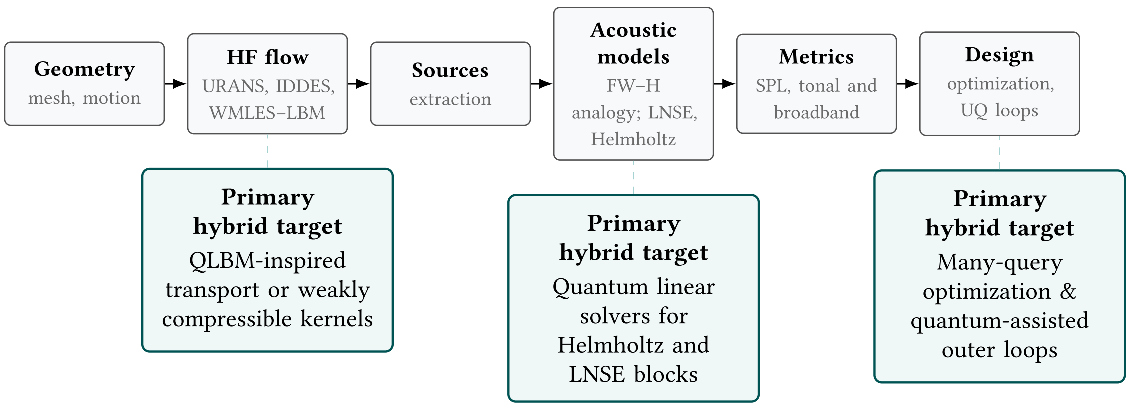

Figure 9: Decomposed CAA chain with three primary hybrid insertion targets shown in the lower shaded callout boxes. These targets are mesoscopic transport near the high-fidelity (HF) flow stage, where unsteady Reynolds-averaged Navier–Stokes (URANS), IDDES, and WMLES–LBM can appear as classical comparators, linearized acoustic modeling through Helmholtz- and LNSE-type blocks or FW–H analogy, and outer-loop design or many-query optimization with uncertainty quantification (UQ) loops. Geometry, source extraction, and metrics remain largely classical in the near-term discussion.

7.2 Decomposed Workflows and Candidate Insertion Points

Aeroacoustics is often discussed as a demanding application for quantum CFD because of turbulence, broadband content, and long time horizons. At the same time, engineering CAA is typically already split into unsteady flow, extraction of source or surface data, and acoustic propagation or reconstruction via analogies, linearized equations, or frequency-domain models. For rotating machinery, FW–H and Farassat-type formulations convert unsteady blade loading and surface-pressure data into far-field acoustic predictions [21,136]. Related moving-source acoustic-analogy formulations provide additional context for source propagation in uniformly moving media [137]. That decomposition yields well-defined interfaces at which hybrid quantum–classical acceleration has been hypothesized in the broader QCFD literature, without assuming that an entire propeller-noise prediction will run on a quantum processor.

Classical studies of propeller tip-vortex noise, tonal noise in centrifugal fans, and liner acoustics coupled through linearized Navier–Stokes/Helmholtz formulations exemplify the same workflow structure [18,19,22]. Compressor distortion and axial-compressor flow-control studies provide rotating-machinery source-flow and design-loop context, while acoustic radiation should still be treated through dedicated CAA models [138,139]. They anchor the discussion in published CAA practice without prescribing a near-term quantum implementation roadmap.

7.3 Fan and Propeller Studies as Acoustic-Observable Templates

The propeller and fan studies are best used here as acoustic-observable templates for quantities that present QLBM methods have yet to address directly. Axial-fan benchmark studies and ducted-propeller analyses provide additional engineering templates because they combine unsteady flow simulation, source extraction, acoustic propagation, and validation against receiver-side noise metrics [140,141]. Yao et al. studied blade-tip vortex noise for future electric-aircraft propellers using improved delayed detached-eddy simulation (IDDES) coupled with a convective FW–H formulation, with aerodynamic design and noise mitigation treated together [18]. Ottersten et al. studied tonal-noise generation in a voluteless centrifugal fan using IDDES and FW–H, where the inlet-gap configuration affected the unsteady flow structures that interact with the rotating blades and contribute to tonal noise [19]. These studies are useful for this review because they identify the flow and acoustic quantities that a future QLBM or hybrid quantum method would need to preserve before it could be considered relevant to engineering CAA.

For a propeller case, the relevant quantities include tip-vortex strength and trajectory, blade-loading fluctuations, near-field pressure data on FW–H source surfaces, and far-field sound-pressure metrics. For a centrifugal-fan case, the corresponding quantities include wall-pressure spectra, blade-passing-frequency content, the location and strength of turbulence and blade-interaction regions, and the far-field tonal response. These requirements are stricter than reproducing a velocity field on a simplified lattice. A quantum or hybrid solver that distorts phase, amplitude, spectral content, or boundary loading would have limited value for CAA, even if the underlying transport benchmark appears accurate.

To connect this discussion to a concrete engineering aeroacoustic problem, Fig. 10 shows a representative propeller blade-tip vortex noise workflow adapted from Yao et al. [18]. It serves here as an acoustic-observable template rather than a quantum-computing result, and it illustrates the full classical chain from source-region vortical structures, through the permeable FW–H data surface and observer placement, to the far-field directivity used to compare designs. These are the same classes of quantities that a future QLBM or hybrid quantum–classical method would need to preserve before it could contribute to engineering CAA.

This example clarifies the intended role of QLBM in the present review. Panel (a) corresponds to the source-region transport problem, where a mesoscopic method must preserve vortex strength, phase, and fluctuation amplitudes. Panel (b) forms the interface between the flow solver and the acoustic analogy, where pressure or loading data are transferred to FW–H-type propagation. Panel (c) gives the engineering output. The QLBM roadmap proposed here therefore complements full propeller-noise prediction, and it identifies which source-region, readout, and hybrid-propagation blocks should be benchmarked first. Table 5 summarizes the corresponding fan, propeller, and liner observable templates used for this comparison.

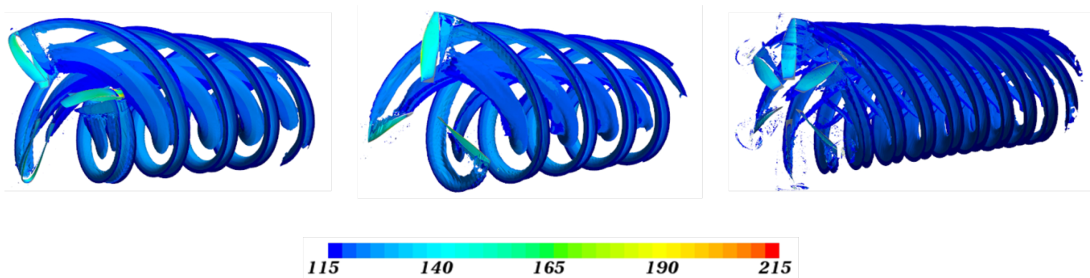

a Source-region tip-vortex structures.

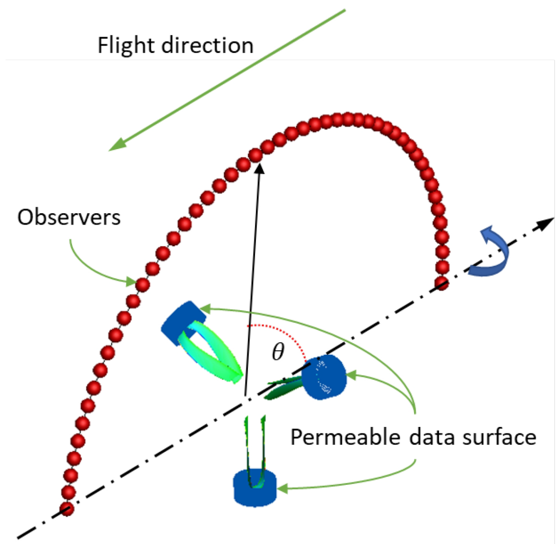

b FW–H data surface and observers.

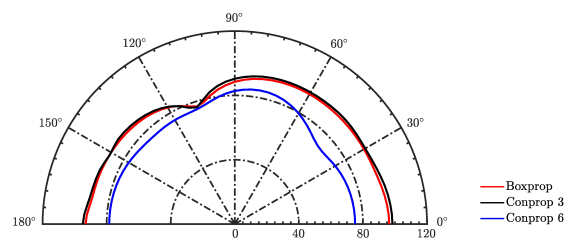

c Far-field OASPL directivity.

Figure 10: Representative engineering aeroacoustic workflow for propeller blade-tip vortex noise, adapted from Yao et al. [18]. Panel (**a**) shows tip-vortex and source-region structures visualized as Q-criterion iso-surfaces colored by velocity magnitude for three propeller designs (Boxprop, Conprop 3, and Conprop 6). Panel (**b**) shows the permeable FW–H data surface and the far-field observer arc, together with the flight direction and emission angle θ used for the acoustic prediction. Panel (**c**) shows the far-field OASPL directivity for the same designs, the receiver-side acoustic quantity used to compare them. The figure defines the real acoustic observables that a future QLBM or hybrid quantum–classical method must preserve, namely source-region vortical structures, pressure and loading data on acoustic source surfaces, and receiver-side directivity or spectra.

Table 5: Fan, propeller, and liner studies used as acoustic-observable templates for evaluating QLBM and hybrid quantum methods. The purpose is to define source-relevant and receiver-relevant observables for future evaluation, while keeping present engineering CAA cases as classical reference workflows.

Anchor Case	Classical CAA Structure	Quantities a QLBM or Hybrid Method Would Need to Preserve
Electric-aircraft propeller noise [18]	IDDES flow solution coupled to convective FW–H acoustic prediction	Tip-vortex strength and trajectory; blade-loading fluctuations; near-field pressure on FW–H source surfaces; far-field SPL and tonal or broadband spectral content

(Continued)

Table 5 (continued)

Anchor Case	Classical CAA Structure	Quantities a QLBM or Hybrid Method Would Need to Preserve
Voluteless centrifugal-fan tonal noise [19]	IDDES flow solution coupled to FW–H acoustic prediction	Wall-pressure spectra; blade-passing-frequency peak; turbulence and blade-interaction location; sensitivity to inlet-gap or geometry changes; far-field tonal response
Liner and duct propagation [22]	Coupled LNSE and Helmholtz-type propagation with viscothermal and boundary effects	Frequency-domain pressure field; impedance or liner boundary response; attenuation and phase accuracy; receiver-side acoustic metrics

In this setting, QLBM belongs at the mesoscopic transport and source-region level once it recovers pressure fluctuations, non-equilibrium stresses, wall data, and spectra with acceptable fidelity. Hybrid quantum linear solvers fit more naturally into Helmholtz or LNSE-type propagation once a classical flow simulation has supplied the source data. The fan and propeller studies define the acoustic observables against which any future QLBM or hybrid method must be judged.

7.4 Three Distinct Quantum Routes through CAA

The workflow view separates three different quantum routes that should be evaluated with different criteria. This separation is important because QLBM, quantum linear solvers, and quantum-assisted optimization address different parts of an aeroacoustic pipeline.

1. **QLBM route for weakly compressible transport and source-region physics.** QLBM is primarily connected to the mesoscopic part of the problem, including weakly compressible transport, reduced source-region dynamics, moment recovery, and simplified acoustic-source models. In this route, the central question is whether the method preserves pressure fluctuations, velocity fluctuations, non-equilibrium stresses, wall-pressure data, and spectra with sufficient fidelity for CAA.
2. **Hybrid quantum linear-solver route for acoustic propagation.** Acoustic propagation, liner response, and duct acoustics often lead to Helmholtz, LNSE, or coupled LNSE–Helmholtz systems [22,142,143]. These problems are closer to sparse linear algebra than to full nonlinear turbulent flow. We therefore identify hybrid quantum linear solvers as candidate kernels for propagation or frequency-domain blocks, with classical CFD or LBM supplying the acoustic sources. The relevant quantum linear-system foundations are provided by HHL and subsequent quantum linear-system algorithm developments [29,45], while CFD-oriented hybrid studies provide the application context [30–33].
3. **Quantum-assisted design route for repeated low-noise design loops.** Low-noise fan and propeller design often requires many geometry changes, parameter sweeps, uncertainty studies, and optimization loops. Quantum annealing, quadratic unconstrained binary optimization (QUBO) formulations, the quantum approximate optimization algorithm (QAOA), and quantum-inspired or hybrid optimization may become useful for such outer-loop tasks, including geometry optimization, source localization, sensor placement, reduced-order calibration, and uncertainty quantification, while the high-fidelity IDDES, LES, or LBM forward solve remains classical [144–146].

This three-route structure avoids treating QLBM as the only quantum connection to aeroacoustics. QLBM belongs mainly to mesoscopic transport and source-region modeling. Hybrid quantum linear solvers belong mainly to propagation and frequency-domain acoustics. Quantum-inspired optimization belongs mainly to repeated design and uncertainty workflows. Table 6 summarizes this division across relevant CFD and CAA subproblems.

Table 6: Qualitative mapping of CFD/CAA subproblems to classical practice, plausible quantum or hybrid routes, and horizon, including deep neural network (DNN) wall models, PINN wall models, Reynolds-averaged Navier–Stokes (RANS), UQ in design loops, and reduced-order models (ROM). The last column indicates how each subproblem typically appears in aeroacoustics and rotating-machinery CAA.

CFD Subproblem	Classical Methods Today	Possible Quantum or Hybrid Route	Horizon	Main Bottleneck	Aeroacoustics and Rotating Machinery
Unsteady turbulent carrier flow (LES/IDDES/RANS)	HPC CFD, wall models, LES/IDDES/RANS; LBM-LES in selected mesoscopic stacks	Mostly classical; quantum unlikely to replace bulk solver soon	Long	Nonlinearity, BCs, readout	Source flow for FW–H; dominates cost in many studies
Weakly compressible and mesoscopic transport	LBM, mesoscopic weakly compressible schemes, hybrid transport models	QLBM kernels; hybrid collision–stream splits	Near–mid	Encoding, unitary collision, BC realism	Relevant to installed propulsion/duct paths; weakly compressible noise [114–117]
Acoustic analogy and propagation	FW–H, wave extrapolation	Classical methods lead; quantum role secondary	Long	I/O of surfaces, signal chain	Core to propeller/fan noise workflows [18,19]
Linear acoustics, Helmholtz, and LNSE blocks	FEM/BEM, coupled LNSE–Helmholtz	VQLS and QLSA on sparse blocks; hybrid frequency solves [29,31–33,147]	Near–mid	Preconditioning, state prep, readout	Liners, ducting, installed noise [22]
ROM, surrogates, and data-driven closure	DNN/PINN wall models [79,85]	Quantum-inspired tensors; hybrid sampling [41]	Near–mid	Training data, transferability	Design loops, many-query scenarios
Outer-loop optimization and UQ	Adjoints, gradient sampling	Quantum-assisted optimization (limited)	Near–mid	Problem encoding, noise	Blade/geometry sweeps for tonal noise [18,19]

7.5 Realism and Present Limits

At present, existing QLBM methods fall short of industrial propeller or fan aeroacoustics. The realistic near-term question is narrower. It asks whether selected quantum, hybrid, or quantum-inspired kernels can accelerate subproblems inside classical CAA workflows. Full fan or propeller noise prediction still requires turbulent source generation, complex geometry, moving boundaries, wall-pressure and loading spectra, acoustic propagation, and receiver-side metrics. These requirements remain beyond current QLBM demonstrations.

This realism is consistent with the QLBM literature reviewed above. Advection–diffusion QLBM studies remain valuable because they test encoding, collision, streaming, and time marching, but they remain transport benchmarks instead of engineering aeroacoustic solvers [13,15]. Dynamic-circuit work addresses the important time-marching problem by reducing the need for full step-by-step reinitialization, yet it remains part of a longer path toward practical CFD and CAA usage [50]. Nonlinear QLBM work is a major advance because it moves beyond purely linear transport, but industrial CAA also requires boundary realism, source spectra, wall data, and comparison with optimized classical LBM and CFD baselines [16].

Accordingly, QLBM is best assessed as a mesoscopic kernel for selected transport and source-region tasks, hybrid quantum linear solvers on Helmholtz, LNSE, liner, and duct propagation blocks, and quantum-assisted optimization in repeated low-noise design loops.

8 Alternative Quantum Entry Points beyond QLBM: Linearized Acoustics and Helmholtz-Type Blocks

QLBM is only one possible route for connecting quantum algorithms with aeroacoustic workflows. Frequency-domain acoustics, liner and duct acoustics, and coupled LNSE and Helmholtz formulations often lead to sparse linear systems or repeated linear solves inside outer loops. Duct and liner acoustics often reduce to frequency-domain Helmholtz, LNSE, or coupled propagation problems with impedance and viscothermal boundary effects [142,143,148]. We therefore identify these problem classes as candidate test cases for hybrid quantum linear solvers; this is a proposed research direction rather than an established quantum-acoustics result. Quantum linear-system algorithms provide the foundation for sparse linear solves [29,45]. High-precision differential-equation and PDE algorithms extend this foundation to time-dependent and spectral problem settings [149–152]. CFD-oriented hybrid studies provide the application context [31–33]. Na et al. proposed a unified approach that couples the LNSE and Helmholtz equations to predict sound propagation with viscothermal losses in acoustic liners [22]. Such a formulation provides a concrete classical comparator for quantum-accelerated or hybrid linear algebra, without requiring a full quantum Navier–Stokes solve.

For installed propulsion and noise-control components, this line of work is strategically important because it identifies a credible target for hybrid quantum methods. Locally linear acoustic propagation with engineering boundary physics is narrower than full turbulent CFD, but it remains directly connected to practical CAA workflows. Fan-duct and liner studies in particular suggest that quantum acceleration should first be evaluated on well-defined propagation or frequency-domain subproblems rather than on complete turbulent fan or propeller simulations [23,142,143]. Important open issues remain, including state preparation when boundary data or acoustic sources enter the linear system, frequency-by-frequency or multi-frequency outer loops, boundary-condition fidelity, and comparison with modern classical sparse solvers and preconditioners. Even with these limitations, the target is well aligned with the hybrid QCFD view that quantum methods are more likely to enter through selected subproblems than through monolithic flow solvers.

9 Classical MRT-LBM Acoustic Multipole Benchmark

This section describes a D3Q19 MRT-LBM acoustic benchmark for harmonic monopole, dipole, and quadrupole radiation in a quiescent weakly compressible lattice. Sound is generated by an additive particle source term inserted after MRT collision and before streaming. The construction uses source moments in the spirit of additive LBM multipole methods [24], while the macroscopic reference below is derived independently for the implemented D3Q19 MRT collision model. The domain is cubic and sufficiently large that the observer arrays lie in the far field of the compact source; the simulation is run for a fixed number of timesteps chosen so that the outgoing wave has not yet reached the boundary when acoustic quantities are extracted. The benchmark serves two roles. It validates the classical solver against an MRT-derived Chapman–Enskog macroscopic multipole reference, and it defines the collision, source, streaming, and readout blocks that are carried forward in the QLBM uplift of Section 10. It is not intended as a full-scale fan or propeller noise simulation; rather, it is a controlled CAA-relevant rung between idealized QLBM demonstrations and the more demanding installed-flow benchmarks required for engineering use. Fig. 11 shows the domain layout, observer geometry, and update workflow.

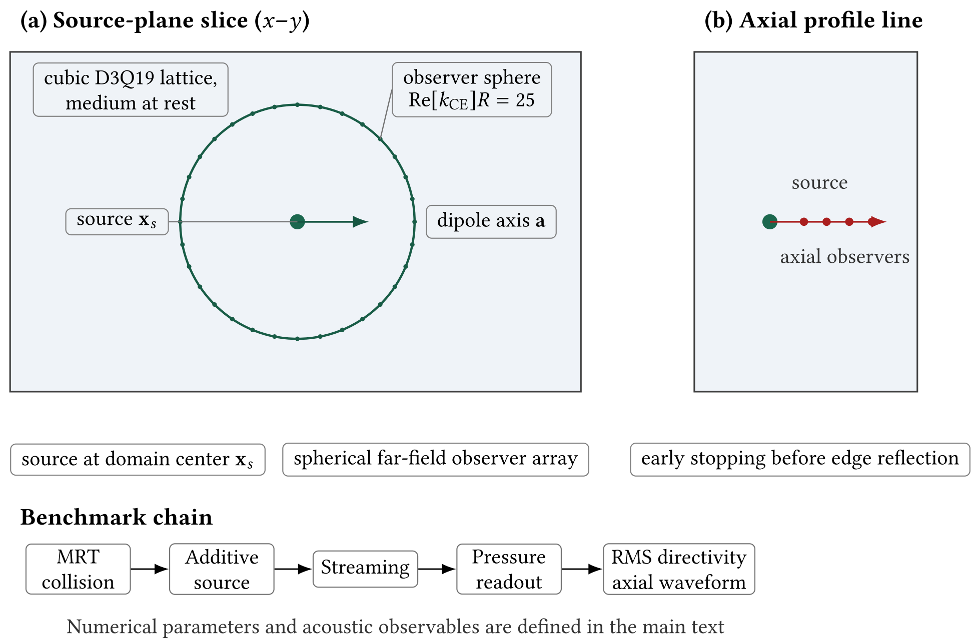

Figure 11: Computational setup for the three-dimensional, D3Q19 multiple-relaxation-time (MRT) lattice Boltzmann method (MRT-LBM) acoustic multipole benchmark. Panel (**a**) shows a central slice through the cubic lattice, with the compact harmonic source at the domain center, a spherical directivity observer array at a nominal radius R satisfying the Chapman–Enskog (CE) reference-wavenumber relation $\mathrm{Re}[k_{\mathrm{CE}}(\omega)]R = 25$, and the dipole axis $\mathbf{a}$. Panel (**b**) shows the orthogonal slice with the source location, the axial line used for the signed source-moment density-fluctuation profile $\rho'/\mathcal{M}$, and the dipole-axis direction. The medium is at rest. The workflow strip summarizes MRT collision, additive source insertion, periodic streaming, and acoustic readout based on root-mean-square (RMS) directivity.

Throughout this section, $\rho'(\mathbf{x}, t) = \rho(\mathbf{x}, t) - \rho_0$ denotes the density fluctuation about the uniform base density.

The validation uses two complementary acoustic observables. The signed axial density-fluctuation response $\rho'/\mathcal{M}$ checks the radiated wave along the propagation direction, including wavelength, phase, and amplitude, and the root-mean-square (RMS) directivity checks the angular radiation pattern on a spherical observer array placed in the far field. Together, these quantities probe both the propagation accuracy and the spatial radiation pattern of the lattice, and provide a compact classical reference for the later quantum formulation.

9.1 MRT-LBM Update Used in the Benchmark

Let $f_i(\mathbf{x}, t)$ denote the population associated with lattice velocity $\mathbf{c}_i$, where $i = 0, \ldots, N_q - 1$. For the D3Q19 lattice used here, $N_q = 19$. The present benchmark uses an MRT collision model because moment-space relaxation gives additional control over hydrodynamic and non-hydrodynamic modes. Three-dimensional MRT formulations with D3Q15 and D3Q19 velocity sets provide the classical basis for this choice [109,153]. The MRT collision is written in moment space as

$$\mathbf{m} = \mathsf{M}\mathbf{f}, \tag{10}$$

$$\mathbf{m}^{\star} = \mathbf{m} - \Lambda\left(\mathbf{m} - \mathbf{m}^{eq}\right), \tag{11}$$

$$\mathbf{f}^{\star} = \mathsf{M}^{-1}\mathbf{m}^{\star}. \tag{12}$$

Here M is the moment transform, Λ is the diagonal relaxation matrix, and $\mathbf{m}^{eq}$ is the equilibrium moment vector. The relaxation parameter reported in Table 7 sets the viscous relaxation scale inside the MRT matrix, while conserved and non-hydrodynamic modes are handled through the diagonal entries of Λ. Streaming then shifts each post-collision population along its discrete velocity:

$$f_i(\mathbf{x} + \mathbf{c}_i\Delta t, t + \Delta t) = f_i^{\star}(\mathbf{x}, t). \tag{13}$$

The acoustic pressure fluctuation is recovered from the density fluctuation through the weakly compressible relation

$$p'(\mathbf{x}, t) = c_s^2\left[\rho(\mathbf{x}, t) - \rho_0\right]. \tag{14}$$

9.2 Periodic Streaming and Multipole Source

Post-collision populations are streamed periodically along the discrete lattice velocities. The domain size and timestep count are chosen so that the outgoing acoustic field is sampled before periodic wrap-around reaches the observers. This deliberate simplification isolates source insertion, MRT dispersion, waveform recovery, and directivity, but it does not test wall, absorbing, impedance, or open-boundary treatments. Table 7 lists the grid, relaxation parameter, forcing frequency, source amplitude, observer locations, and post-processing window used in the simulations below.

The monopole, dipole, and quadrupole sources follow acoustic source-term LBM formulations in which sound is generated by additive particle or source terms at the population level and validated against analytical acoustic fields [24,154,155]. The source is inserted after collision and before streaming,

$$f_i^{\star}(\mathbf{x}, t) \;\leftarrow\; f_i^{\star}(\mathbf{x}, t) + s_i(\mathbf{x}, t), \tag{15}$$

so that the multipole character is defined entirely through the velocity moments of the source,

$$\mathcal{S}^{(0)} = \sum_i s_i, \qquad \mathcal{S}_\alpha^{(1)} = \sum_i c_{i\alpha}\, s_i, \qquad \mathcal{S}_{\alpha\beta}^{(2)} = \sum_i c_{i\alpha} c_{i\beta}\, s_i, \tag{16}$$

where $\mathcal{S}^{(0)}$ is the mass (monopole) source, $\mathcal{S}_\alpha^{(1)}$ is the momentum (dipole) source, and $\mathcal{S}_{\alpha\beta}^{(2)}$ is the stress (quadrupole) source. For the implemented D3Q19 MRT scheme, Taylor expansion followed by Chapman–Enskog expansion gives the source-modified linear conservation laws [109,122,153]

$$\partial_t \rho' + \partial_\alpha j_\alpha = \mathcal{S}^{(0)} - \frac{1}{2}\left(\partial_t \mathcal{S}^{(0)} + \partial_\alpha \mathcal{S}_\alpha^{(1)}\right), \tag{17}$$

$$\partial_t j_\alpha + c_s^2 \partial_\alpha \rho' - \mathcal{V}_\alpha = \left(1 - \frac{1}{2}\partial_t\right)\mathcal{S}_\alpha^{(1)} - \partial_\beta\left(T_{\alpha\beta\gamma\delta}\mathcal{S}_{\gamma\delta}^{(2)}\right) + c_s^2\left(\tau_e - \frac{1}{2}\right)\partial_\alpha \mathcal{S}^{(0)}. \tag{18}$$

Here

$$T_{\alpha\beta\gamma\delta} = \tau_v P_{\alpha\beta\gamma\delta}^{dev} + \tau_e P_{\alpha\beta\gamma\delta}^{tr},$$

so the deviatoric quadrupole part relaxes with τ_v, while the trace part relaxes with the MRT energy-mode time $\tau_e = 1/s_1$. This is the D3Q19 MRT-specific Chapman–Enskog result used in the analytical reference.

The source acts at a single lattice node, consistent with a compact point source. Its spatial profile is a normalized point envelope centered at $\mathbf{x}_s$,

$$g(\mathbf{x}) = \delta_{\mathbf{x},\mathbf{x}_s}, \qquad \sum_{\mathbf{x}} g(\mathbf{x}) = 1, \tag{19}$$

where $\delta_{\mathbf{x},\mathbf{x}_s}$ is the Kronecker delta on the lattice. The envelope localizes the source to a single node; the multipole character is set by the discrete velocity weights. Using the lattice weights w_i, the lattice sound speed c_s, a unit dipole axis $\mathbf{a}$, and a symmetric quadrupole tensor $\mathbf{Q}$, the source term is built in Hermite form on the D3Q19 lattice as

$$s_i^{\text{mono}}(\mathbf{x}, t) = w_i\, \sigma_0(t)\, g(\mathbf{x}), \tag{20}$$

$$s_i^{\text{dip}}(\mathbf{x}, t) = w_i\, \frac{\mathbf{c}_i \cdot \mathbf{a}}{c_s^2}\, \sigma_1(t)\, g(\mathbf{x}), \tag{21}$$

$$s_i^{\text{quad}}(\mathbf{x}, t) = w_i\, \frac{c_{i\alpha} c_{i\beta} Q_{\alpha\beta} - c_s^2 \operatorname{tr} \mathbf{Q}}{2c_s^4}\, \sigma_2(t)\, g(\mathbf{x}). \tag{22}$$

These satisfy $\sum_i c_{i\alpha} s_i^{\text{mono}} = 0$, so the monopole injects mass with no net momentum; $\sum_i s_i^{\text{dip}} = 0$ with $\sum_i c_{i\alpha} s_i^{\text{dip}} = \sigma_1(t)\, g(\mathbf{x})\, a_\alpha$, so the dipole injects momentum along $\mathbf{a}$ with no net mass; and the quadrupole term carries the prescribed stress moment $\mathcal{S}_{\alpha\beta}^{(2)}$ with vanishing mass and momentum, realizing the lowest three multipoles of the D3Q19 source-moment decomposition.

The source strengths are modulated harmonically with a smooth start-up ramp that suppresses the initial transient,

$$\sigma_0(t) = \sigma_1(t) = \sigma_2(t) = A\, r(t)\, \sin(\omega t), \qquad r(t) = \begin{cases} \dfrac{1}{2}\left[1 - \cos(\pi t/T)\right], & 0 < t < T, \\ 1, & t \geq T, \end{cases} \tag{23}$$

where A is the source amplitude, ω is the angular frequency, and $T = 2\pi/\omega$ is one forcing period.

Table 7: Numerical parameters for the classical MRT-LBM acoustic multipole validation. All quantities are given in lattice units.

Category	Parameter	Value
Domain and lattice	Grid and velocity set	$192 \times 192 \times 192$ D3Q19 lattice
Solver	Collision model, relaxation time, and density	MRT-LBM, $\tau = 0.505$, $\rho_0 = 1.0$
Solver	Time integration and precision	160 time steps with early stopping, double precision
Medium	Background state	Medium at rest, $\mathbf{u}_0 = \mathbf{0}$ (no mean flow)
Source location	Source center (all cases)	$\mathbf{x}_s = (96, 96, 96)$
Source frequency and shape	Harmonic forcing and spatial profile	$f = 0.045$, $\omega = 2\pi f$, single-node point source
Monopole source	Source amplitude	$A = 10^{-6}$
Dipole source	Amplitude and dipole axis	$A = 10^{-6}$, $\mathbf{a} = (1, 0, 0)$
Quadrupole source	Amplitude and tensors	$A = 10^{-6}$; longitudinal (Q_{xx}) and shear (Q_{xy})
Directivity observers	Far-field radius and angular sampling	$\mathrm{Re}[k_{\mathrm{CE}}]R = 25$; 19×72 angular samples
Axial profile	Direction and range	x-axis, $\lvert\mathbf{x} - \mathbf{x}_s\rvert$ up to 80 lattice units
Post-processing	Sampling and harmonic recovery	Validation from step 110; least-squares single-tone fit

In all three multipole cases, $A = 10^{-6}$, so the generated density and pressure perturbations remain in the linear acoustic regime. Nonlinear acoustic effects are therefore negligible at the scale of the present benchmark; the retained response is the $O(A)$ radiated field, while quadratic corrections scale as $O(A^2)$.

9.3 Validation Observables

The validation compares the lattice acoustic field against an MRT-derived Chapman–Enskog macroscopic reference. Accurate acoustic verification requires preserving weak pressure fluctuations, their radiated waveform, and their angular pattern at low numerical dissipation [122–124]. The source construction uses the same additive population-source moment principle as earlier LBM multipole work [24], where $\hat{p}(\mathbf{x})$ is our outgoing Green-function solution of the viscous acoustic wave equation obtained by Chapman–Enskog expansion of the same implemented D3Q19 MRT collision model, relaxation rates (including the fixed energy-mode rate $s_1 = 1.19$), and source moments. The reference wavenumber is

$$k_{\mathrm{CE}}(\omega) = \frac{\omega}{\sqrt{c_s^2 + i\omega\nu_L}}, \qquad \nu_L = \frac{4}{3}\nu + \nu_b, \tag{24}$$

where $\nu = c_s^2(\tau - \frac{1}{2})$ and $\nu_b = \frac{2}{3}c_s^2(\tau_e - \frac{1}{2})$ with $\tau_e = 1/s_1$. The observer radius is set by $\mathrm{Re}[k_{\mathrm{CE}}(\omega)]R = 25$. This CE reference gives the macroscopic limit of the implemented lattice scheme; the exact finite-wavelength forced lattice resolvent lies outside this comparison. In harmonic form the analytic field is

$$p'(\mathbf{x}, t) = \Re\left\{\hat{p}(\mathbf{x})e^{i\omega t}\right\}. \tag{25}$$

Two observables are used. The first, and main, observable is the signed axial density-fluctuation response along the propagation direction, normalized by the scalar source moment $\mathcal{M}$ of each multipole. We use

$$\mathcal{M}_0 = \mathcal{S}^{(0)}, \qquad \mathcal{M}_x = \mathbf{e}_x \cdot \mathcal{S}^{(1)}, \qquad \mathcal{M}_{xx} = \mathcal{S}^{(2)}_{xx}, \tag{26}$$

and plot

$$\frac{\rho'(\mathbf{x})}{\mathcal{M}}, \qquad \mathcal{M} \in \{\mathcal{M}_0, \mathcal{M}_x, \mathcal{M}_{xx}\}, \tag{27}$$

which places the monopole, dipole, and quadrupole on a common scale and compares the radiated waveform directly. This quantity is equivalent to $p'(\mathbf{x})/(c_s^2\mathcal{M})$ through $p' = c_s^2\rho'$. The second observable is the RMS directivity on the far-field observer sphere,

$$p_{\mathrm{rms}}^{(\chi)}(\theta, \varphi) = \frac{\left|\hat{p}_\chi(\mathbf{x}_s + R\mathbf{n}(\theta, \varphi))\right|}{\sqrt{2}}, \qquad \chi \in \{\mathrm{mono}, \mathrm{dip}, \mathrm{quad}\}. \tag{28}$$

The agreement with the analytic pattern is summarized by the shape correlation

$$\tilde{p}_{\mathrm{rms}}(\theta, \varphi) = p_{\mathrm{rms}}(\theta, \varphi) - \bar{p}_{\mathrm{rms}}, \tag{29}$$

$$C_{\mathrm{dir}} = \frac{\langle \tilde{p}_{\mathrm{rms}}^{LBM}, \tilde{p}_{\mathrm{rms}}^{ana} \rangle}{\|\tilde{p}_{\mathrm{rms}}^{LBM}\|_2 \, \|\tilde{p}_{\mathrm{rms}}^{ana}\|_2}, \tag{30}$$

where $\bar{p}_{\mathrm{rms}}$ is the mean over the observer sphere. The amplitude at each observer is obtained from a least-squares single-tone fit of the sampled pressure history, taken over a post-transient window that begins after the source ramp has completed and the wavefront has passed the observers. The directivity panels are normalized by each curve's own peak so that they isolate the angular radiation shape.

9.4 Benchmark Results

The main benchmark comparison is shown in Fig. 12, which compares the signed, source-moment-normalized axial density-fluctuation response $\rho'/\mathcal{M}$ of the lattice with the analytic point-source reference for the monopole, dipole, and quadrupole. Normalizing each response by its scalar source moment ($\mathcal{M}_0$, $\mathcal{M}_x$, $\mathcal{M}_{xx}$) puts the three multipoles on a common axis and isolates the radiated waveform. Across all three panels the lattice (MRT-LBM) reproduces the wavelength and phase of the analytic oscillation essentially exactly along the propagation direction. The peak amplitudes match closely.

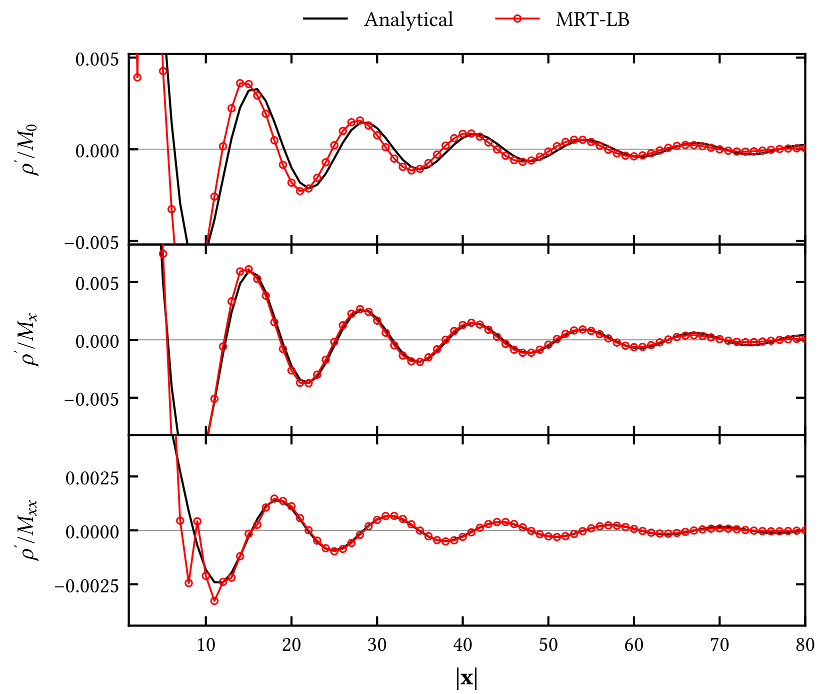

Figure 12: Main benchmark comparison for the classical MRT-LBM acoustic multipole setup. Each panel shows the signed, source-moment-normalized axial density-fluctuation response $\rho'/\mathcal{M}$ as a function of distance $|\mathbf{x}|$ from the source, for the monopole ($\rho'/\mathcal{M}_0$), dipole ($\rho'/\mathcal{M}_x$), and quadrupole ($\rho'/\mathcal{M}_{xx}$). The lattice result (MRT-LBM, markers) is compared with the MRT-derived Chapman–Enskog macroscopic reference (line); both share the same absolute normalization, so wavelength, phase, and amplitude are compared directly. The lattice matches the analytic wavelength and phase across the full range, with only small residual amplitude differences at larger distances.

Fig. 13 shows the corresponding RMS pressure directivity on the far-field observer sphere for four source configurations. The monopole gives near-isotropic radiation, the dipole and the xx quadrupole give the expected two-lobe patterns with the correct null structure, and the xy quadrupole gives the characteristic four-lobe clover pattern. In every case the lattice markers track the analytic reference around the full ring.

Table 8 reports the directivity-shape correlation between the lattice and analytic patterns for the four source configurations over the post-transient sampling window.

Taken together, the axial waveform comparison and the directivity patterns confirm that the setup reproduces both the radiated waveform and the angular radiation structure of the analytic multipoles, with directivity correlations above 0.999 for the directional cases. This gives a compact, well-controlled classical acoustic reference for the QLBM uplift.

The benchmark gives a compact classical target for the QLBM uplift in Section 10. Collision, source injection, streaming, pressure readout, and acoustic recovery enter as separate algorithmic blocks.

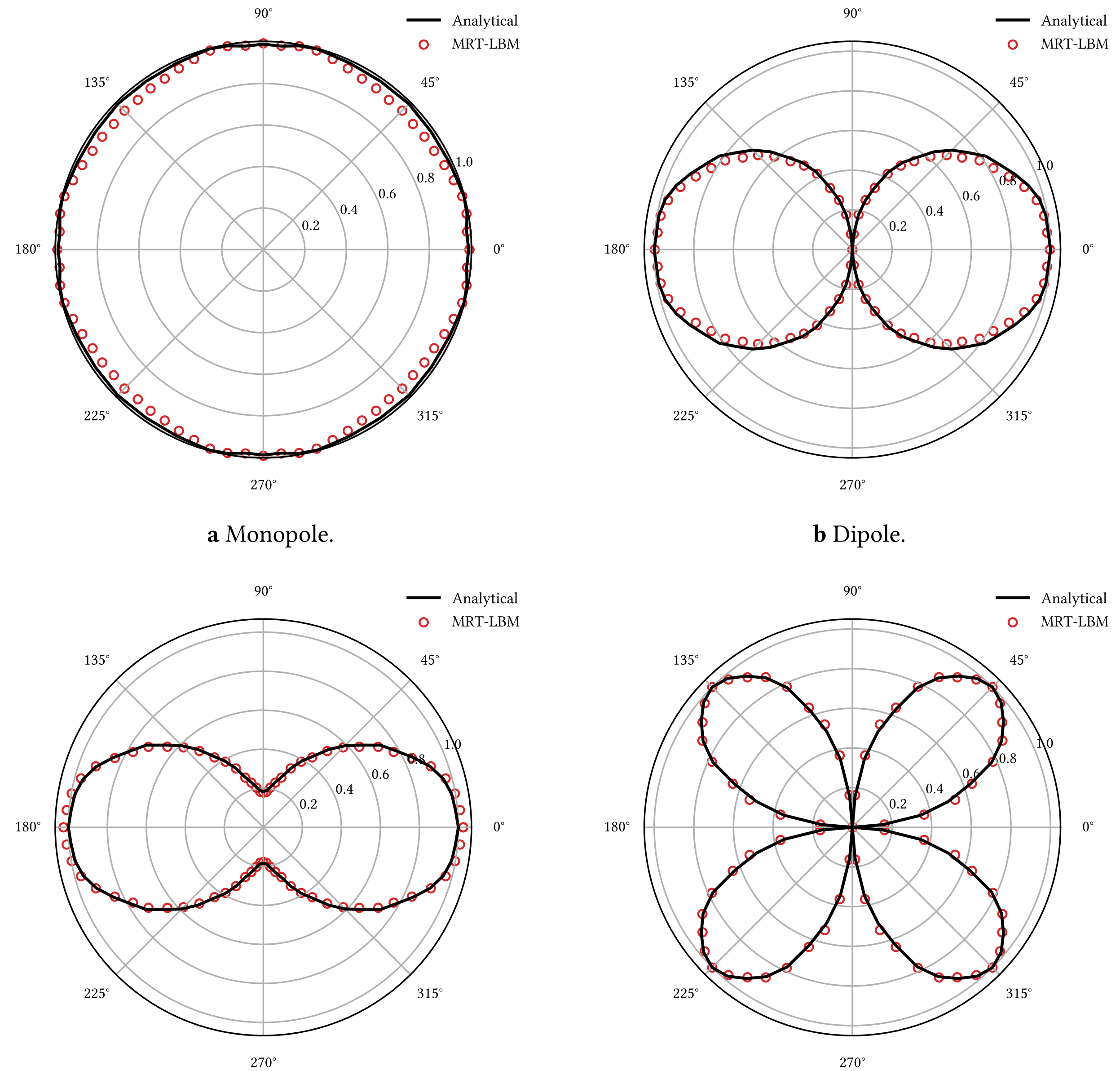

a Monopole.

b Dipole.

c Quadrupole (xx).

d Quadrupole (xy).

Figure 13: RMS pressure directivity for the classical MRT-LBM acoustic benchmark on the far-field observer ring at a nominal radius R satisfying $\mathrm{Re}[k_{\mathrm{CE}}(\omega)]R = 25$. Each panel compares the lattice result (markers) with the MRT-derived Chapman–Enskog macroscopic reference (line) for the monopole, dipole, xx quadrupole, and xy quadrupole, with each curve normalized to its own peak to compare the radiation shape.

Table 8: Directivity-shape agreement for the classical MRT-LBM acoustic multipole benchmark on the 192^3 lattice, evaluated over the post-transient sampling window (from step 110). The correlation measures the agreement between the lattice and analytic RMS radiation patterns on the far-field observer sphere at a nominal radius R satisfying $\mathrm{Re}[k_{\mathrm{CE}}(\omega)]R = 25$. The monopole pattern is isotropic, so a shape correlation is not informative and the uniform radiation is verified directly from the directivity panel instead.

Case	Directivity Correlation	Comment
Monopole	Isotropic pattern	Uniform radiation reproduced
Dipole	0.9996	Two-lobe pattern and axial null
Quadrupole (xx)	0.9991	Lateral two-lobe quadrupole pattern
Quadrupole (xy)	0.9996	Four-lobe clover pattern

10 Illustrative QLBM Uplift of the MRT-LBM Acoustic Benchmark Using Mainstream Linear-Algebraic Encodings

This section is an illustrative operator-level uplift, rather than an executed quantum implementation. No quantum circuit is compiled or simulated, and no numerical qubit, gate, depth, or shot counts are claimed. The purpose is to identify how the validated classical MRT-LBM acoustic benchmark would decompose into state preparation, lifted collision–source operators, streaming, and acoustic readout, so that future QLBM implementations can report resources in a reproducible way.

The classical benchmark of Section 9 exposes the pieces that a quantum lattice Boltzmann formulation must represent, including local MRT collision, compact acoustic source insertion, streaming, and acoustic readout. This section gives a general-to-specific mathematical uplift of that benchmark into an illustrative QLBM architecture using Carleman lifting, SVD-based unitary dilation, and conditional streaming [16,17,52,156,157], together with LCU and block encoding [46,147]. The section defines a concrete benchmark architecture on which state preparation, lifted-operator construction, streaming, and measurement assumptions can be discussed using the same physical quantities as the classical MRT-LBM acoustic problem.

10.1 General Operator-Level QLBM Representation

Collect all D3Q19 populations over the computational lattice into a global vector $\mathbf{f}(t) = \{f_i(\mathbf{x}, t)\}_{\mathbf{x},i} \in \mathbb{R}^{NN_q}$, where $N = N_x N_y N_z$ and $N_q = 19$. The classical MRT-LBM acoustic update of Section 9 can then be written abstractly as

$$\mathbf{f}^{n+1} = \mathcal{S}_{\mathrm{str}}\mathcal{F}^{\chi}_{\mathrm{src}}(t_n)\mathcal{C}_{\mathrm{MRT}}(\mathbf{f}^n), \qquad \chi \in \{\mathrm{mono}, \mathrm{dip}, \mathrm{quad}\}. \tag{31}$$

Here $\mathcal{C}_{\mathrm{MRT}}$ is the MRT collision, $\mathcal{F}^{\chi}_{\mathrm{src}}$ is the monopole, dipole, or quadrupole forcing, and $\mathcal{S}_{\mathrm{str}}$ is the velocity-conditioned periodic streaming shift. Eq. (31) follows the same operator order as the reference solver: collision, source insertion, and streaming.

The quantum uplift is written at the operator level. The non-unitary or affine collision–source part of the update is first represented by a lifted linear operator $\mathcal{A}^{\chi}(t_n)$. A unitary realization of this lifted operator may then be obtained through LCU, block encoding, SVD-based unitary dilation, or a related hybrid construction. At the schematic level,

$$|\Psi^{n+1}\rangle \propto U_{\mathrm{str}} U_{\mathcal{A}^{\chi}(t_n)} |\Psi^n\rangle. \tag{32}$$

The streaming shift U_{str} is unitary on the periodic lattice, so no separate boundary operator appears. This is a direct benefit of the periodic, early-stopping benchmark: the only non-unitary content is the collision–source map $\mathcal{A}^{\chi}(t_n)$, and the rest of the timestep is an exact unitary shift.

$$(\langle 0|_a \otimes I)U_{\mathcal{A}}(|0\rangle_a \otimes I) = \frac{\mathcal{A}^{\chi}(t_n)}{\alpha}, \qquad \alpha \geq \|\mathcal{A}^{\chi}(t_n)\|. \tag{33}$$

Eq. (33) defines a block encoding of the generally non-unitary lifted operator [46]. If the operator admits an efficient decomposition as a linear combination of implementable unitaries, it may be realized probabilistically using an LCU construction [147]. SVD-based unitary dilation provides an alternative used in QLBM-oriented constructions [17]. Quantum linear-system algorithms such as HHL are relevant when the computational task is formulated as solving a linear system, but they do not by themselves provide a generic implementation of the collision–source map [29,45,158]. These operator-embedding approaches are consistent with recent QLBM formulations that handle non-unitary collision operators through SVD-based or related decomposition strategies and conditional streaming constructions [17,51,62]. They are also consistent with Carleman-lattice-Boltzmann (CLB) constructions, which use sparse lifted matrices, matrix-oracle access, and block-encoding techniques to represent lifted or nonlinear dynamics [52,54,156]. The matrix-oracle CLB formulation also makes clear that ancilla overhead and success probability remain serious obstacles for multi-step time evolution [156].

10.2 Carleman-Lifted Realization for the MRT-LBM Acoustic Benchmark

Carleman linearization provides a natural route for representing polynomial nonlinear dynamics as a truncated linear system, and it has become central in quantum algorithms for dissipative nonlinear differential equations, related linear or nonlinear ordinary differential equation (ODE) models, and recent multi-step QLBM formulations based on local Carleman lifting [157,159,160]. For the present weakly compressible acoustic benchmark, a concrete realization is obtained by expanding the MRT-LBM update around the quiescent base state used in the classical simulation:

$$\rho = \rho_0 + \rho', \qquad \mathbf{u} = \mathbf{u}', \qquad |\rho'|/\rho_0 \ll 1, \tag{34}$$

so that the base state is the medium at rest, $\mathbf{u}_0 = \mathbf{0}$, and $\mathbf{u}'$ is the acoustic velocity fluctuation.

Using the moment-space MRT update defined in Section 9.1, with $\mathbf{m} = \mathsf{M}\mathbf{f}$, diagonal relaxation matrix Λ, and equilibrium moments $\mathbf{m}^{eq}$, the uplift is formulated in terms of perturbations about the same quiescent base state. Define the perturbation variable

$$\mathbf{y} = \mathbf{m} - \bar{\mathbf{m}}, \tag{35}$$

where $\bar{\mathbf{m}}$ is the base-state moment vector. Under acoustic scaling, the local collision map can be expressed schematically as a polynomial map

$$\mathbf{y}^{+} = A_1\mathbf{y} + A_2(\mathbf{y} \otimes \mathbf{y}) + A_3(\mathbf{y} \otimes \mathbf{y} \otimes \mathbf{y}) + \cdots + \mathbf{b}^{\chi}(t_n), \tag{36}$$

where $\mathbf{b}^{\chi}(t_n)$ collects the known affine pieces from source insertion. For a Carleman truncation of order K, introduce the lifted vector

$$\mathbf{z}_K = \left[1,\ \mathbf{y},\ \mathbf{y}^{\otimes 2},\ \ldots,\ \mathbf{y}^{\otimes K}\right]^T. \tag{37}$$

The nonlinear or affine MRT-LBM step is then approximated by a linear lifted update

$$\mathbf{z}_K^{n+1} \approx \mathcal{A}_K^{\chi}(t_n)\mathbf{z}_K^{n}, \qquad \chi \in \{\text{mono}, \text{dip}, \text{quad}\}. \tag{38}$$

The role of $K = 2$ is different from the role of the linear acoustic reference. Because the imposed source amplitudes are small, the benchmark response is assessed in the linear acoustic regime, for which the retained operator is the A_1 part of Eq. (36); a $K = 1$ lift is sufficient for that strictly linear perturbation model. The illustrative uplift, however, is written for the expanded MRT collision map before discarding the second-order equilibrium contribution. Since the standard weakly compressible MRT equilibrium contains quadratic momentum products, $K = 2$ is included as the minimal Carleman truncation that can retain the $A_2(\mathbf{y} \otimes \mathbf{y})$ term. Thus, $K = 2$ is used as a reporting option for the weakly nonlinear MRT collision structure, rather than as a requirement for the linear acoustic validation.

The monopole, dipole, and quadrupole sources enter through the additive particle source term $s_i^{\chi}(\mathbf{x}, t)$ defined in Section 9.2, with $\chi \in \{\text{mono}, \text{dip}, \text{quad}\}$. The corresponding population update is an affine forcing map,

$$\mathbf{f} \mapsto \mathbf{f} + \mathbf{s}^{\chi}(\mathbf{x}, t), \tag{39}$$

whose conserved velocity moments $\mathcal{S}^{(0)}$, $\mathcal{S}_{\alpha}^{(1)}$, and $\mathcal{S}_{\alpha\beta}^{(2)}$ prescribe the monopole, dipole, and quadrupole strengths directly. In the lifted Carleman system, this source enters as a known coefficient block inside $\mathcal{A}_K^{\chi}(t_n)$. Fig. 14 shows the general-to-specific uplift architecture for this benchmark.

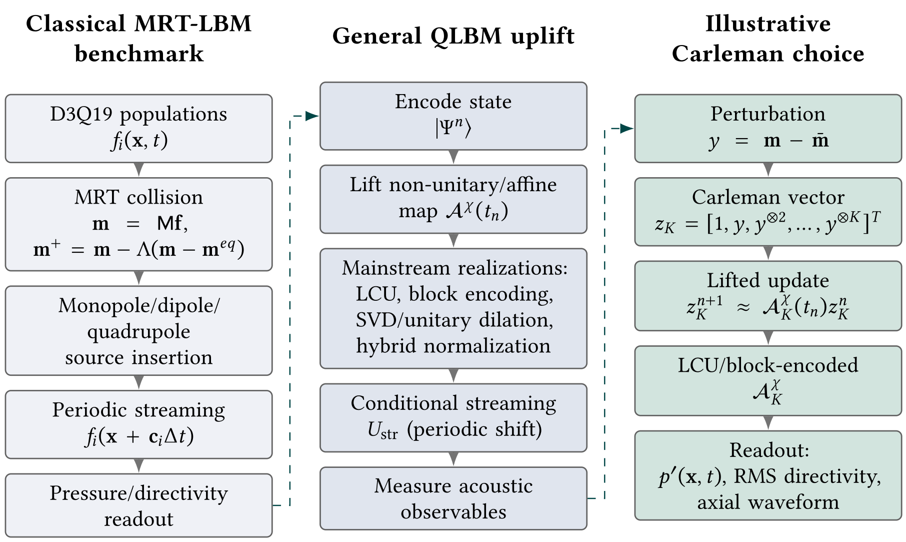

Figure 14: General-to-specific QLBM uplift of the MRT-LBM acoustic benchmark. The left column shows the classical D3Q19 MRT-LBM workflow used for the monopole, dipole, and quadrupole acoustic validation, following the reference solver order of MRT collision, source insertion, periodic streaming, and pressure/directivity readout. The middle column shows the general quantum-algorithmic representation, where the non-unitary or affine collision–source part is lifted into a linear operator and represented using mainstream linear-algebraic tools such as linear combination of unitaries (LCU), block encoding, SVD-based unitary dilation, or hybrid normalization, followed by conditional streaming and measurement of acoustic observables. The right column shows the illustrative Carleman realization, in which perturbation variables are lifted into $\mathbf{z}_K = [1, \mathbf{y}, \mathbf{y}^{\otimes 2}, \ldots, \mathbf{y}^{\otimes K}]^T$, evolved by $\mathcal{A}_K^{\chi}(t_n)$, followed by conditional streaming and measurement of the axial waveform and RMS directivity. The schematic defines a benchmark architecture for future resource analysis without claiming present quantum advantage.

10.3 LCU, Block Encoding, and Streaming

The quantum state encodes the lifted LBM vector, including Carleman degree as well as physical populations.

$$|\Psi_K^n\rangle = \frac{1}{\|\mathbf{z}_K^n\|} \sum_{\alpha} z_{K,\alpha}^n |\alpha\rangle, \tag{40}$$

where α indexes the position, velocity or moment component, and Carleman degree. The dominant quantum task is to apply the generally non-unitary lifted operator $\mathcal{A}_K^{\chi}(t_n)$. A standard route is to construct an LCU or block encoding

$$\mathcal{A}_K^{\chi}(t_n) = \sum_{\ell=0}^{L-1} a_\ell(t_n) U_\ell, \tag{41}$$

with unitary components U_ℓ and coefficients a_ℓ, or equivalently a unitary $U_{\mathcal{A}_K^{\chi}}$ satisfying Eq. (33) with normalization $\alpha_K \geq \|\mathcal{A}_K^{\chi}(t_n)\|$. An LCU realization is probabilistic and may use ancilla post-selection [147]; amplitude amplification and modern block-encoding or quantum singular-value-transformation techniques belong to the broader framework [46]. The LCU and block-encoding components of the proposed uplift are consistent with the broader Hamiltonian-simulation and matrix-transformation literature, including truncated Taylor-series simulation, qubitization, quantum singular value transformation, and linear combination of Hamiltonian simulation methods for non-unitary dynamics [46,161–164]. This is the quantum-linear-algebraic representation of collision and source insertion.

Periodic streaming is represented by the lattice shift

$$U_{\text{str}}|\mathbf{x}\rangle|i\rangle = |(\mathbf{x} + \mathbf{c}_i \Delta t) \bmod \mathbf{L}\rangle|i\rangle, \tag{42}$$

where $\mathbf{L} = (L_x, L_y, L_z)$ is the domain size in lattice units. On a quantum register this shift is unitary, so streaming enters the uplift without additional block-encoding overhead; the non-unitary part of the timestep is confined to the lifted collision–source operator. In the present benchmark the simulation horizon is short enough that boundary wrap does not affect the sampled region.

A compact timestep summary is therefore

$$|\Psi_K^{n+1}\rangle \propto U_{\text{str}} U_{\mathcal{A}_K^{\chi}(t_n)} |\Psi_K^n\rangle, \qquad c \in \{\text{mono}, \text{dip}, \text{quad}\}, \tag{43}$$

on the same periodic 192^3 lattice used in the classical benchmark. The $K = 1$ case corresponds to the linearized acoustic perturbation operator, whereas $K = 2$ is the minimal lift that retains the first quadratic contribution of the expanded MRT collision map.

10.4 Acoustic Observables and Benchmark Interpretation

The acoustic observables are recovered from the physical-population component of the lifted state. The density and pressure fluctuation are

$$\rho(\mathbf{x}, t) = \sum_{i=0}^{18} f_i(\mathbf{x}, t), \qquad \rho'(\mathbf{x}, t) = \rho(\mathbf{x}, t) - \rho_0, \qquad p'(\mathbf{x}, t) = c_s^2 \rho'(\mathbf{x}, t). \tag{44}$$

The benchmark-level observables are the signed axial density-fluctuation response $\rho'/\mathcal{M}$ along the propagation direction and the RMS directivity on the observer sphere, at the same observer locations used in the classical MRT-LBM validation of Section 9.3:

$$p_{\mathrm{rms,QLBM}}(\theta,\varphi) \quad \text{against} \quad p_{\mathrm{rms,ana}}(\theta,\varphi), \tag{45}$$

and

$$\rho'_{\mathrm{QLBM}}(\mathbf{x})/\mathcal{M} \quad \text{against} \quad \rho'_{\mathrm{ana}}(\mathbf{x})/\mathcal{M}. \tag{46}$$

These are compared against the MRT-derived Chapman–Enskog monopole, dipole, and quadrupole references and against the classical MRT-LBM results. The key performance quantities for the QLBM uplift include directivity correlation, axial-waveform error, and the Carleman truncation order K, the block-encoding normalization α_K, post-selection success probability, state preparation cost, number of timesteps before re-normalization or readout, and the measurement budget required to recover the acoustic observables. For this benchmark, observer amplitudes, RMS directivity, and selected spectral quantities could be estimated with amplitude-estimation routines, where the useful speedup depends on state preparation cost, repeated operator application, and measurement precision [165–167]. For a time-marched acoustic benchmark, the repeated operator-application cost, normalization, success probability, condition-number dependence, and measurement of selected observables should be reported explicitly, as emphasized across modern quantum linear-system and time-dependent differential-equation solvers [45,46,152,158,164].

The construction is an illustrative benchmark architecture for future resource analysis. A meaningful QLBM resource claim should report logical qubits, gate depth, state-preparation assumptions, qRAM or oracle access, measurement budget, amplitude-estimation overhead, error-correction assumptions, and physical resource estimates [96,168]. Its cost depends on the Carleman truncation order K, sparsity and conditioning of $\mathcal{A}_K^{\chi}$, block-encoding normalization α_K, state-preparation assumptions, post-selection or amplitude-amplification overhead, number of timesteps, and the measurement budget required to recover acoustic observables. Non-unitary collision and source operations enter as lifted linear or affine maps represented through LCU, block encoding, SVD-based dilation, or hybrid normalization, tied throughout to the classical acoustic problem introduced earlier. Fig. 15 is therefore used as a reporting template for the acoustic uplift, using the fixed classical parameters in Table 7; it identifies the quantities that a future circuit realization or hardware-aware emulator should report.

11 Research Directions for QLBM in Engineering CFD

The following directions summarize recurring themes in the QLBM literature and in broader QCFD reviews, emphasizing practical constraints, acoustic observables, and staged validation over speculative quantum advantage.

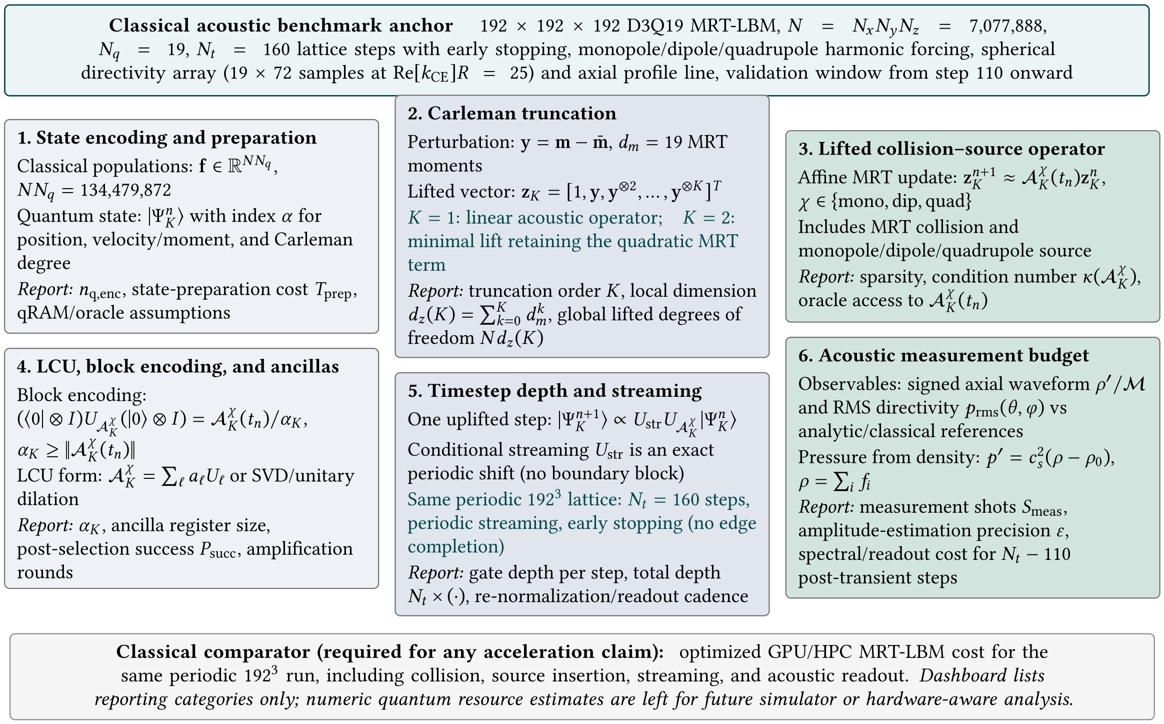

Figure 15: Resource-accounting reporting template for the illustrative QLBM uplift of the MRT-LBM acoustic benchmark. The anchor row records fixed classical parameters from Table 7. Panels 1–6 list the encoding, Carleman truncation, lifted collision–source operator, block encoding, timestep, and acoustic-measurement quantities that a future circuit realization or hardware-aware emulator should report before any QLBM acceleration claim is compared with optimized classical MRT-LBM or LBM–CAA baselines. The state-preparation panel includes quantum random access memory (qRAM) or oracle assumptions. Symbolic scaling expressions are tied to the notation in Section 10; numerical quantum qubit, gate, depth, and shot counts are intentionally left for future implementation-specific analysis.

11.1 Benchmark Hierarchy

Based on the literature synthesized above, Table 1 makes explicit a ladder that the narrative sections of this paper have already assumed implicitly, progressing from linear ADE transport through canonical flow benchmarks, then mesoscopic weakly compressible transport-acoustics (LBM-native) and, separately, linearized wave-propagation acoustics aligned with hybrid linear solvers, and finally turbulence stress tests, before arguing about engineering aeroacoustics. Without such a hierarchy, cross-paper comparison stays ambiguous. Explicit placement on the ladder, together with classical comparators matched to the same stage of difficulty, makes claims easier to interpret and contest on common ground.

The acoustic multipole benchmark in Section 9, together with the QLBM uplift in Section 10, provides a concrete example of a weakly compressible acoustic benchmark on this ladder. It links the review discussion to a reproducible MRT-LBM test with additive source injection, axial-waveform and directivity recovery, and an explicit lifted-operator and block-encoding decomposition.

Future work should implement the proposed QLBM acoustic formulation in a quantum-circuit simulator or hardware-aware emulation framework, and should compare the resulting directivity, axial waveform, measurement cost, and resource scaling against the classical MRT-LBM reference.

11.2 A Small CAA-Oriented Benchmark Set

The benchmark ladder in Table 1 can be made more actionable by adding a small set of demonstrative CAA benchmarks. The classical acoustic multipole case in Section 9 and its illustrative uplift in Section 10 form the first member of this set. These cases test whether a QLBM, hybrid quantum linear solver, or quantum-inspired workflow preserves the acoustic quantities that matter before extending the discussion to full fan or propeller noise prediction. The proposed cases are simpler than industrial geometries, yet each one targets a specific acoustic weakness in quantum-fluid discussions, including recovery of pressure fluctuations, spectral accuracy, boundary treatment, state preparation, and readout.

The first case is one-dimensional acoustic-pulse propagation. It tests whether a weak pressure or density disturbance can be propagated with the correct wave speed, amplitude, phase, dispersion, attenuation, and reflection behavior. This case is closest to the LBM-acoustics connection because pressure follows from density fluctuations in the weakly compressible lattice setting. The second case is a two-dimensional cylinder or edge dipole-source surrogate. A classical flow solver can provide wall-pressure or compact-source data, while the acoustic propagation step is handled separately. This case tests whether source-region quantities such as wall-pressure spectra, phase, and compact dipole strength are preserved. The third case is a duct or liner Helmholtz benchmark. This case is aimed less at QLBM and more at hybrid quantum linear solvers, because the main object is a sparse frequency-domain system with impedance or liner boundary conditions. Table 9 summarizes these demonstrative CAA benchmarks and the specific acoustic weakness targeted by each case.

Table 9: Small CAA-oriented benchmark set for evaluating QLBM, hybrid quantum linear solvers, and quantum-inspired workflows. The cases are demonstrative validation targets rather than full industrial aeroacoustic simulations.

Benchmark	Main Acoustic Quantities	Suitable Quantum Route	Success Criteria
1D acoustic pulse propagation	$\rho'(x,t)$, $p'(x,t)$, lattice sound speed c_s, phase, dispersion, attenuation, reflection	QLBM or weakly compressible LBM-like transport	Correct wave speed, stable amplitude, controlled numerical dispersion, and accurate reflection from simple boundaries.
2D cylinder or edge dipole-source surrogate	Wall-pressure signal, compact dipole strength, phase, source spectrum, near-field pressure	Classical flow with QLBM-inspired or hybrid source-region kernel	Preserved source frequency, amplitude, phase, wall-pressure spectrum, and source-location sensitivity.
Duct or liner Helmholtz problem [22]	Frequency-domain pressure field, impedance response, attenuation, phase, receiver-side SPL	Hybrid quantum linear solver, VQLS, QLSA, or quantum Krylov-type block [29,31–33,147]	Clear state-preparation model, credible preconditioning, accurate impedance boundary response, and efficient readout of receiver metrics.

These benchmarks also clarify the division between the three quantum routes identified in Section 7. QLBM is best tested on the acoustic-pulse and source-region transport cases. Hybrid quantum linear solvers are better tested on the Helmholtz or LNSE-type duct and liner case. Quantum-inspired optimization becomes relevant only after these forward models have reliable observables, since optimization without acoustic fidelity would only accelerate an unreliable design loop.

11.3 Boundary-Condition Realism

Boundary treatment should be treated as a primary validation target rather than a secondary implementation detail. Further attention to bounce-back, immersed boundaries, wall models, moving boundaries, and frequency-domain acoustic boundary conditions would narrow a persistent gap relative to mature classical LBM practice and would strengthen the path toward engineering relevance. For acoustics-oriented QLBM, the boundary question is especially important because wall pressure, reflected waves, impedance effects, and source-surface data can directly affect phase, amplitude, spectra, and directivity. Future QLBM studies should therefore report not only whether a boundary rule can be encoded, but also whether the resulting acoustic observables remain accurate over many time steps.

11.4 Resource Accounting

Cross-study comparison is easier when asymptotic complexity is reported together with its dependence on sparsity, conditioning, precision, and the assumed matrix-access model. Quantum linear-system and block-encoding analyses make these algorithmic dependencies explicit [45,46,158]. Time-dependent differential-equation and high-precision PDE algorithms further show that temporal discretization, target accuracy, and state or output assumptions must be included in complexity assessments [152,164]. Practical assessments also emphasize that formal speedups are insufficient without qubit count, gate count and depth, measurement requirements, state-preparation assumptions, classical preprocessing, and hardware-level resource costs [96,168]. For the acoustic uplift, Fig. 15 makes the same reporting categories explicit at benchmark level. As the literature grows, such accounting increasingly functions as expected context alongside numerical results.

11.5 Advanced Classical Baselines and Data-Driven Closures

Where industrial or deployment-oriented claims appear, baselines drawn from GPU-accelerated classical LBM, data-driven LBM wall models, and established hybrid CFD/CAA pipelines carry particular interpretive weight. Such baselines are important because classical LBM is already highly optimized for local streaming–collision updates, parallel execution, wall modeling, and aeroacoustic post-processing. A QLBM result should therefore be compared against a classical method matched to the same benchmark rung, observable, and accuracy requirement, rather than against a minimal or unoptimized reference implementation.

The recent convergence of LBM with data-driven wall modeling, broader machine-learning methods for fluid mechanics, reinforcement-learning wall models, and automated turbulence-closure discovery suggests a longer-term possibility [169–171]. Quantum and machine-learning accelerators could both be inserted into an LBM-centric engineering workflow. Whether such programs can outperform highly optimized classical HPC remains an open question. It can only be settled through head-to-head studies on agreed benchmark ladders and comparable classical baselines.

12 Research Roadmap

This closing roadmap identifies measurable benchmark targets that connect the QLBM literature surveyed here to aeroacoustic and low-noise propulsion workflows. It complements the methodological checklist in Section 11.

First, hybrid quantum–classical linear solvers should be tested on LNSE–Helmholtz or Helmholtz-type propagation blocks with duct, liner, or radiation-boundary conditions, using established classical formulations as baselines [22,31–33]. Useful reporting targets are residual reduction, phase error, amplitude error, boundary-condition error, preconditioning cost, state-preparation assumptions, readout cost, and comparison with optimized classical sparse solvers.

Second, QLBM benchmarks should progress from scalar advection–diffusion toward weakly compressible acoustic transport and source-region tests. The MRT-LBM monopole, dipole, and quadrupole benchmark in Section 9 is a suitable first target because it has explicit reference observables: axial waveform error, RMS directivity error, source-amplitude scaling, lattice-dispersion error, timestep count, and measurement budget. A future circuit or hardware-aware emulator should report Carleman order and truncation assumptions because they determine the size and approximation error of the lifted system [157,159]. Block-encoding normalization and state-preparation assumptions should be stated explicitly for the chosen nonunitary implementation, while time-marching cost should be reported for time-dependent solvers [163,164]. Hardware-level reporting should include logical qubits, gate depth, shot count, and execution-time assumptions [168]. Wall-clock performance should then be compared with matched GPU or HPC LBM baselines that reflect validated turbulence and wall-modeling workflows [78,85].

Third, boundary and workflow realism should become explicit benchmark stages. After the present periodic-domain acoustic test, natural extensions are absorbing or radiation boundaries, impedance boundaries, wall-pressure readout, and source-surface coupling to FW–H or LNSE propagation. Longer-term CAA relevance should be judged by receiver-side quantities such as spectra, phase, directivity, and sound-pressure level, rather than by internal circuit evolution alone. Outer-loop blade or fan design studies may then provide practical hybrid targets, with quantum annealing, QUBO formulations, QAOA, quantum-inspired, or hybrid methods used for selected reduced-order, optimization, inverse-design, or uncertainty-quantification blocks while the main IDDES, LES, or LBM flow solve remains classical.

13 Conclusions

Quantum CFD has moved beyond a purely speculative topic, yet it remains far from industrial maturity. Credible near-term strategies are hybrid and selective, targeting linear or block-linear bottlenecks while leaving most nonlinear fluid dynamics on classical hardware. Within this broader landscape, quantum lattice Boltzmann methods draw sustained attention because LBM offers a mesoscopic algorithmic structure that is often amenable to decomposition into quantum-friendly pieces.

The QLBM literature has evolved from early advection–diffusion formulations to more complete and more ambitious programs addressing Navier–Stokes-like dynamics, unitary collision operators, dynamic circuits, boundary handling, and even nonlinear turbulence-oriented formulations. Yet the same literature also reveals the magnitude of the remaining obstacles, including nonlinearity, measurement cost, state preparation, and the need for comparison against highly optimized classical LBM.

From an engineering viewpoint, a plausible role for QLBM is the gradual emergence of hybrid strategies for selected kernels within broader simulation pipelines, instead of immediate replacement of mature CFD or aeroacoustic workflows. Industrial CAA for fans, propellers, and installed configurations is standardly organized as a decomposed flow–acoustics chain. The literature on fan noise, propeller noise, and linearized acoustics supplies worked examples of subproblems that the QCFD community has discussed as possible targets for selective hybridization.

The classical MRT-LBM acoustic multipole benchmark included in this paper makes this staged view more concrete, and the illustrative QLBM uplift shows how the same acoustic calculation can be mapped to a mainstream lifted-operator architecture. In that decomposition, non-unitary collision and source operations are treated as lifted linear or affine maps that may be represented through LCU, block encoding, SVD-based dilation, or hybrid normalization, while streaming remains an exact periodic shift and acoustic validation is based on the radiated axial waveform and RMS directivity against the MRT-derived Chapman–Enskog macroscopic reference. This gives the review a defined benchmark target for future resource accounting.

Making progress comparable across research groups will require shared benchmark ladders, realistic boundary treatments, transparent resource accounting, explicit readout models, and comparisons with optimized classical baselines. These are the same elements emphasized in Section 6 and in the checklist framed there. Viewed in this light, QLBM remains a research bridge between quantum algorithm design and engineering CFD. Its main value is to connect mesoscopic modeling with hybrid high-performance workflows, and to move present quantum fluid algorithms from proof-of-concept demonstrations toward the validation standards expected in application-driven simulation.

Acknowledgement: Not applicable.

Funding Statement: This research was funded by Vinnova–Fordonsstrategisk forskning och innovation (FFI) in the project "3D Virtual Platform for Digitalization of Holistic Acoustic Environment in Cabs of Heavy-Duty Vehicles (OCTAVE)" under Grant No. P2024-01011.

Author Contributions: Muhammad Idrees Khan: conceptualization, methodology, code, validation, formal analysis, investigation, writing, and visualization. Hua-Dong Yao: conceptualization, methodology, supervision, review, and editing. All authors reviewed and approved the final version of the manuscript.

Availability of Data and Materials: The numerical parameters, and post-processed data used to generate the MRT-LBM acoustic multipole benchmark figures are available from the corresponding author upon reasonable request.

Ethics Approval: Not applicable.

Conflicts of Interest: The authors declare no conflicts of interest.

References

1. Arksey H, O'Malley L. Scoping studies: towards a methodological framework. Int J Soc Res Methodol. 2005;8(1):19–32. doi:10.1080/1364557032000119616.
2. Snyder H. Literature review as a research methodology: an overview and guidelines. J Bus Res. 2019;104(5):333–9. doi:10.1016/j.jbusres.2019.07.039.
3. Tricco AC, Lillie E, Zarin W, O'Brien KK, Colquhoun H, Levac D, et al. PRISMA extension for scoping reviews (PRISMA-ScR): checklist and explanation. Ann Internal Med. 2018;169(7):467–73. doi:10.7326/M18-0850.
4. Page MJ, McKenzie JE, Bossuyt PM, Boutron I, Hoffmann TC, Mulrow CD, et al. The PRISMA 2020 statement: an updated guideline for reporting systematic reviews. BMJ. 2021;372:n71. doi:10.1136/bmj.n71.
5. Rethlefsen ML, Kirtley S, Waffenschmidt S, Ayala AP, Moher D, Page MJ, et al. PRISMA-S: an extension to the PRISMA statement for reporting literature searches in systematic reviews. Syst Rev. 2021;10(1):39. doi:10.1186/s13643-020-01542-z.
6. Donthu N, Kumar S, Mukherjee D, Pandey N, Lim WM. How to conduct a bibliometric analysis: an overview and guidelines. J Bus Res. 2021;133(5):285–96. doi:10.1016/j.jbusres.2021.04.070.
7. Malinverno G, Blasco Alberto J. A review of the current state-of-the-art of quantum computing for CFD: approaches, advantages, and limitations. Aerotecnica Missili Spazio. 2026;105(2):251–68. doi:10.1007/s42496-025-00269-1.
8. Meng ZY, Lu Z, Xiong SY, Zhao YM, Yang Y. Advances in quantum computing for fluid dynamics. Adv Mech. 2025;55(3):541–66. (In Chinese). doi:10.6052/1000-0992-24-041.

9. Amaral CA, Oliveira VL, Salazar JPLC, Duzzioni EI. A review of quantum machine learning and quantum-inspired applied methods to computational fluid dynamics. Braz J Phys. 2025;56(1):39. doi:10.1007/s13538-025-01959-8.
10. Jaksch D, Givi P, Daley AJ, Rung T. Variational quantum algorithms for computational fluid dynamics. AIAA J. 2023;61(5):1885–94. doi:10.2514/1.J062426.
11. Succi S. The lattice Boltzmann equation for fluid dynamics and beyond. Oxford, UK: Oxford University Press; 2001. doi:10.1093/oso/9780198503989.001.0001.
12. Krüger T, Kusumaatmaja H, Kuzmin A, Shardt O, Silva G, Viggen EM. The lattice Boltzmann method: principles and practice. Cham, Switzerland: Springer; 2017. doi:10.1007/978-3-319-44649-3.
13. Budinski L. Quantum algorithm for the advection-diffusion equation simulated with the lattice Boltzmann method. Quantum Inf Process. 2021;20(2):57. doi:10.1007/s11128-021-02996-3.
14. Budinski L. Quantum algorithm for the Navier–Stokes equations by using the streamfunction-vorticity formulation and the lattice Boltzmann method. Int J Quantum Inf. 2022;20(2):2150039. doi:10.1142/S0219749921500398.
15. Wawrzyniak D, Winter J, Schmidt S, Indinger T, Janßen CF, Schramm U, et al. A quantum algorithm for the lattice-Boltzmann method advection-diffusion equation. Comput Phys Commun. 2025;306(1):109373. doi:10.1016/j.cpc.2024.109373.
16. Wang B, Meng Z, Zhao Y, Yang Y. Quantum lattice Boltzmann method for simulating nonlinear fluid dynamics. npj Quantum Inf. 2025;11(1):196. doi:10.1038/s41534-025-01142-6.
17. Liu Z, Benzi J, Emerson DR. Quantum lattice Boltzmann method based on linear equilibrium distribution functions. Front Mech Eng. 2026;11:1717775. doi:10.3389/fmech.2025.1717775.
18. Yao HD, Huang Z, Davidson L, Niu J, Chen ZW. Blade-tip vortex noise mitigation traded-off against aerodynamic design for propellers of future electric aircraft. Aerospace. 2022;9(12):825. doi:10.3390/aerospace9120825.
19. Ottersten M, Yao HD, Davidson L. Inlet gap effect on aerodynamics and tonal noise generation of a voluteless centrifugal fan. J Sound Vib. 2022;540:117304. doi:10.1016/j.jsv.2022.117304.
20. Lighthill MJ. On sound generated aerodynamically. I. General theory. Proc Royal Soc London Ser A Math Phys Sci. 1952;211(1107):564–87. doi:10.1098/rspa.1952.0060.
21. Ffowcs Williams JE, Hawkings DL. Sound generation by turbulence and surfaces in arbitrary motion. Philosop Trans Royal Soc A. 1969;264(1151):321–42. doi:10.1098/rsta.1969.0031.
22. Na W, Yao HD, Boij S, Kabral R, Bodén H, Efraimsson G. A unified approach coupling linearized Navier–Stokes equations and Helmholtz equations to predict sound propagation with viscothermal losses in acoustic liners. Preprint. 2023. doi:10.31224/2976.
23. Wang M, Freund JB, Lele SK. Computational prediction of flow-generated sound. Ann Rev Fluid Mech. 2006;38(1):483–512. doi:10.1146/annurev.fluid.38.050304.092036.
24. Viggen EM. Acoustic multipole sources for the lattice Boltzmann method. Phys Rev E. 2013;87(2):023306. doi:10.1103/PhysRevE.87.023306.
25. Ray N, Banerjee T, Nadiga B, Karra S. Towards solving the Navier–Stokes equation on quantum computers. arXiv:1904.09033. 2019.
26. Griffin KP, Jain SS, Flint TJ, Chan WHR. Investigation of quantum algorithms for direct numerical simulation of the Navier–Stokes equations. Stanford, CA, USA: Center for Turbulence Research, Stanford University; 2019.
27. Gaitan F. Finding flows of a Navier–Stokes fluid through quantum computing. npj Quantum Inf. 2020;6(1):61. doi:10.1038/s41534-020-00291-0.
28. Oz F, Vuppala RKSS, Kara K, Gaitan F. Solving Burgers' equation with quantum computing. Quantum Inf Process. 2022;21(1):30. doi:10.1007/s11128-021-03391-8.
29. Harrow AW, Hassidim A, Lloyd S. Quantum algorithm for linear systems of equations. Phys Rev Lett. 2009;103(15):150502. doi:10.1103/PhysRevLett.103.150502.
30. Chen ZY, Xue C, Chen SM, Lu BH, Wu YC, Ding JC, et al. Quantum approach to accelerate finite volume method on steady computational fluid dynamics problems. Quantum Inf Process. 2022;21(4):137. doi:10.1007/s11128-022-03478-w.
31. Lapworth L. A hybrid quantum-classical CFD methodology with benchmark HHL solutions. arXiv:2206.00419. 2022.

32. Song Z, Deaton R, Gard B, Bryngelson SH. Incompressible Navier–Stokes solve on noisy quantum hardware via a hybrid quantum-classical scheme. Comput Fluids. 2025;288(7965):106507. doi:10.1016/j.compfluid.2024.106507.
33. Chen ZY, Ma TY, Ye CC, Xu L, Bai W, Zhou L, et al. Enabling large-scale and high-precision fluid simulations on near-term quantum computers. Comput Methods Appl Mech Eng. 2024;432(10):117428. doi:10.1016/j.cma.2024.117428.
34. Bharadwaj SS, Sreenivasan KR. Hybrid quantum algorithms for flow problems. Proc Natl Acad Sci. 2023;120(49):e2311014120. doi:10.1073/pnas.2311014120.
35. Meng Z, Yang Y. Quantum computing of fluid dynamics using the hydrodynamic Schrödinger equation. Phys Rev Res. 2023;5(3):033182. doi:10.1103/PhysRevResearch.5.033182.
36. Meena MG, Zhang Y, Jiang W, Lin Y, Gunther S, Gao X. Towards a quantum algorithm for the incompressible nonlinear Navier–Stokes equations. In: Proceedings of the 2024 IEEE International Conference on Quantum Computing and Engineering (QCE); 2024 Sep 15–20; Montreal, QC, Canada. Piscataway, NJ, USA: IEEE; 2024. p. 662–8. doi:10.1109/QCE60285.2024.00083.
37. Li X, Yin X, Wiebe N, Chun J, Schenter GK, Cheung MS, et al. Potential quantum advantage for simulation of fluid dynamics. Phys Rev Res. 2025;7(1):013036. doi:10.1103/PhysRevResearch.7.013036.
38. Gaitan F. Finding solutions of the Navier–Stokes equations through quantum computing. Adv Quantum Technol. 2021;4(10):2100055. doi:10.1002/qute.202100055.
39. Succi S, Itani W, Sanavio C, Sreenivasan KR, Steijl R. Ensemble fluid simulations on quantum computers. Comput Fluids. 2024;270(6):106148. doi:10.1016/j.compfluid.2023.106148.
40. Kumar ED, Frankel SH. Quantum unitary matrix representation of the lattice Boltzmann model for low Reynolds fluid flow simulation. AVS Quantum Sci. 2025;7(1):013802. doi:10.1116/5.0245082.
41. Peddinti RD, Pisoni S, Marini A, Lott P, Argentieri H, Tiunov E, et al. Quantum-inspired framework for computational fluid dynamics. Commun Phys. 2024;7(1):135. doi:10.1038/s42005-024-01623-8.
42. Bharadwaj SS, Sreenivasan KR. Towards simulating fluid flows with quantum computing. Sādhanā. 2025;50(2):57. doi:10.1007/s12046-024-02660-3.
43. Kocherla S, Song Z, Chrit FE, Gard B, Dumitrescu EF, Alexeev A, et al. Fully quantum algorithm for mesoscale fluid simulations with application to partial differential equations. AVS Quantum Sci. 2024;6(3):033806. doi:10.1116/5.0217675.
44. Au-Yeung R, Williams AJ, Kendon VM, Lind SJ. Quantum algorithm for smoothed particle hydrodynamics. Comput Phys Commun. 2024;294:108909. doi:10.1016/j.cpc.2023.108909.
45. Childs AM, Kothari R, Somma RD. Quantum algorithm for systems of linear equations with exponentially improved dependence on precision. SIAM J Comput. 2017;46(6):1920–50. doi:10.1137/16M1087072.
46. Gilyén A, Su Y, Low GH, Wiebe N. Quantum singular value transformation and beyond: exponential improvements for quantum matrix arithmetics. In: Proceedings of the 51st Annual ACM SIGACT Symposium on Theory of Computing, STOC 2019; 2019 Jun 23–26; Phoenix, AZ, USA. New York, NY, USA: ACM; 2019. p. 193–204. doi:10.1145/3313276.3316366.
47. Schalkers MA, Möller M. Efficient and fail-safe quantum algorithm for the transport equation. J Comput Phys. 2024;502(6):112816. doi:10.1016/j.jcp.2024.112816.
48. Xu L, Li M, Zhang L, Sun H, Yao J. Improved quantum lattice Boltzmann method for advection-diffusion equations with a linear collision model. Phys Rev E. 2025;111(4):045305. doi:10.1103/PhysRevE.111.045305.
49. Zeng KY, Niu XD, Khan A, Li DC, Yamaguchi H. A quantum computing-based lattice Boltzmann method with a linearized non-equilibrium collision operator and modular circuit for practical flow simulation. Phys Fluids. 2025;37(8):081701. doi:10.1063/5.0278054.
50. Wawrzyniak D, Winter J, Schmidt S, Indinger T, Janßen CF, Schramm U, et al. Linearized quantum lattice-Boltzmann method for the advection-diffusion equation using dynamic circuits. Comput Phys Commun. 2025;317(15):109856. doi:10.1016/j.cpc.2025.109856.
51. Lee M, Song Z, Kocherla S, Adams A, Alexeev A, Bryngelson SH. A multiple-circuit approach to quantum resource reduction with application to the quantum lattice Boltzmann method. Fut Gener Comput Syst. 2026;174:107975. doi:10.1016/j.future.2025.107975.

52. Sanavio C, Succi S. Lattice Boltzmann–Carleman quantum algorithm and circuit for fluid flows at moderate Reynolds number. AVS Quantum Sci. 2024;6(2):023802. doi:10.1116/5.0195549.
53. Itani W, Sreenivasan KR, Succi S. Quantum algorithm for lattice Boltzmann (QALB) simulation of incompressible fluids with a nonlinear collision term. Phys Fluids. 2024;36(1):017112. doi:10.1063/5.0176569.
54. Sanavio C, Scatamacchia R, De Falco C, Succi S. Three Carleman routes to the quantum simulation of classical fluids. Phys Fluids. 2024;36(5):057143. doi:10.1063/5.0204955.
55. Jennings D, Korzekwa K, Lostaglio M, Mannix P, Ashworth R, Marsili E, et al. Simulating non-trivial incompressible flows with a quantum lattice Boltzmann algorithm. In: AIAA SCITECH 2026 Forum; 2026 Jan 12–16; Orlando, FL, USA. doi:10.2514/6.2026-1936.
56. Bharadwaj SS. QFlowS: quantum simulator for fluid flows. Phys Fluids. 2024;36(10):107112. doi:10.1063/5.0226074.
57. Shinde T, Budinski L, Niemimäki O, Lahtinen V, Liebelt H, Li R. Utilizing classical programming principles in the intel quantum SDK: implementation of quantum lattice Boltzmann method. ACM Trans Quantum Comput. 2025;6(1):9:1–18. doi:10.1145/3678185.
58. Georgescu CA, Schalkers MA, Möller M. QLBM—a quantum lattice Boltzmann software framework. Comput Phys Commun. 2025;315(4):109699. doi:10.1016/j.cpc.2025.109699.
59. Yepez J. Quantum lattice-gas model for computational fluid dynamics. Phys Rev E. 2001;63(4):046702. doi:10.1103/PhysRevE.63.046702.
60. Ingelmann J, Bharadwaj SS, Pfeffer P, Sreenivasan KR, Schumacher J. Two quantum algorithms for solving the one-dimensional advection-diffusion equation. Comput Fluids. 2024;281(1):106369. doi:10.1016/j.compfluid.2024.106369.
61. Tiwari A, Iaconis J, Jojo J, Ray S, Roetteler M, Hill C, et al. Algorithmic advances towards a realizable quantum lattice Boltzmann method. In: Proceedings of the 2025 IEEE International Conference on Quantum Computing and Engineering (QCE); 2025 Aug 31–Sep 5; Albuquerque, NM, USA. Piscataway, NJ, USA: IEEE; 2025. p. 2441–51. doi:10.1109/QCE65121.2025.00265.
62. Lăcătuş MI, Möller M. Surrogate quantum circuit design for the lattice Boltzmann collision operator. Int J Numer Methods Eng. 2026;127(4):e70286. doi:10.1002/nme.70286.
63. Khan MI, Succi S, Yao HD. Deterministic realization of classical dissipation on quantum computers. arXiv:2604.25429. 2026.
64. Steijl R. Quantum circuit implementation of multi-dimensional non-linear lattice models. Appl Sci. 2023;13(1):529. doi:10.3390/app13010529.
65. Bastida-Zamora A, Budinski L, Kerppo O, Lahtinen V, Niemimäki O, Steadman W, et al. Quantum algorithm for the lattice Boltzmann method with applications on real quantum devices. arXiv:2603.02127. 2026.
66. Smagorinsky J. General circulation experiments with the primitive equations: I. The basic experiment. Mon Weather Rev. 1963;91(3):99–164. doi:10.1175/1520-0493(1963)091<0099:GCEWTP>2.3.CO;2.
67. Germano M, Piomelli U, Moin P, Cabot WH. A dynamic subgrid-scale eddy viscosity model. Phys Fluids A. 1991;3(7):1760–5. doi:10.1063/1.857955.
68. Lilly DK. A proposed modification of the Germano subgrid-scale closure method. Phys Fluids A Fluid Dyn. 1992;4(3):633–5. doi:10.1063/1.858280.
69. Eswaran V, Pope SB. An examination of forcing in direct numerical simulations of homogeneous turbulence. Comput Fluids. 1988;16(3):257–78. doi:10.1016/0045-7930(88)90013-8.
70. Guo Z, Zheng C, Shi B. Discrete lattice effects on the forcing term in the lattice Boltzmann method. Phys Rev E. 2002;65(4):046308. doi:10.1103/PhysRevE.65.046308.
71. Chen S, Doolen GD. Lattice Boltzmann method for fluid flows. Ann Rev Fluid Mech. 1998;30(1):329–64. doi:10.1146/annurev.fluid.30.1.329.
72. Aidun CK, Clausen JR. Lattice-Boltzmann method for complex flows. Ann Rev Fluid Mech. 2010;42(1):439–72. doi:10.1146/annurev-fluid-121108-145519.
73. Succi S, Amati G, Benzi R. Challenges in lattice Boltzmann computing. J Stat Phys. 1995;81:5–16. doi:10.1007/BF02179964.

74. Amati G, Succi S, Piva R. Massively parallel lattice-Boltzmann simulation of turbulent channel flow. Int J Modern Phys C. 1997;8(4):869–77. doi:10.1142/S0129183197000746.
75. Eggels JGM. Direct and large-eddy simulation of turbulent fluid flow using the lattice-Boltzmann scheme. Int J Heat Fluid Flow. 1996;17(3):307–23. doi:10.1016/0142-727X(96)00044-6.
76. Yu H, Girimaji SS, Luo LS. Lattice Boltzmann simulations of decaying homogeneous isotropic turbulence. Phys Rev E. 2005;71(1):016708. doi:10.1103/PhysRevE.71.016708.
77. Malaspinas O, Sagaut P. Consistent subgrid scale modelling for lattice Boltzmann methods. J Fluid Mech. 2012;700:514–42. doi:10.1017/jfm.2012.155.
78. Khan MI, Succi S, Falcucci G. Validating the Boltzmann approach to the large-eddy simulations of forced homogeneous incompressible turbulence. Int J Mod Phys C. 2026;164:192. doi:10.1142/S0129183127500641.
79. Khan MI, Succi S, Yao HD, Falcucci G. Physics-constrained neural closure for lattice Boltzmann large-eddy simulation. arXiv:2603.15992. 2026.
80. Tavares HS, Biferale L, Sbragaglia M, Mailybaev AA. Immiscible Rayleigh-Taylor turbulence using mesoscopic lattice Boltzmann algorithms. Phys Rev Fluids. 2021;6(5):054606. doi:10.1103/PhysRevFluids.6.054606.
81. Malaspinas O, Sagaut P. Wall model for large-eddy simulation based on the lattice Boltzmann method. J Comput Phys. 2014;275(1):25–40. doi:10.1016/j.jcp.2014.06.020.
82. Haussmann M, Barreto AC, Kouyi GL, Rivière N, Nirschl H, Krause MJ. Large-eddy simulation coupled with wall models for turbulent channel flows at high Reynolds numbers with a lattice Boltzmann method. Appl Coriolis Mass Flowmeter Comput Math Appl. 2019;78(10):3285–302. doi:10.1016/j.camwa.2019.04.033.
83. Spinelli GG, Gericke J, Masilamani K, Klimach HG. Key ingredients for wall-modeled LES with the lattice Boltzmann method: systematic comparison of collision schemes, SGS models, and wall functions on simulation accuracy and efficiency for turbulent channel flow. Discret Contin Dyn Syst. 2024;17:3224–51. doi:10.3934/dcdss.2023212.
84. Xue X, Yao HD, Davidson L. Wall-modeled large-eddy simulation integrated with synthetic turbulence generator for multiple-relaxation-time lattice Boltzmann method. Phys Fluids. 2023;35(6):065115. doi:10.1063/5.0153526.
85. Xue X, Wang S, Yao HD, Davidson L, Coveney PV. Physics informed data-driven near-wall modelling for lattice Boltzmann simulation of high Reynolds number turbulent flows. Commun Phys. 2024;7(1):338. doi:10.1038/s42005-024-01832-1.
86. Premnath KN, Pattison MJ, Banerjee S. Dynamic subgrid scale modeling of turbulent flows using lattice-Boltzmann method. Phys A Stat Mech Its Appl. 2009;388(13):2640–58. doi:10.1016/j.physa.2009.02.041.
87. Buzzicotti M, Tauzin G. Inertial range statistics of the entropic lattice Boltzmann in 3D turbulence. Phys Rev E. 2021;104(1):015302. doi:10.1103/PhysRevE.104.015302.
88. Obrecht C, Kuznik F, Tourancheau B, Roux JJ. A new approach to the lattice Boltzmann method for graphics processing units. Comput Math Appl. 2011;61(12):3628–38. doi:10.1016/j.camwa.2010.01.054.
89. Lehmann M, Krause MJ, Amati G, Sega M, Harting J, Gekle S. Accuracy and performance of the lattice Boltzmann method with 64-bit, 32-bit, and customized 16-bit number formats. Phys Rev E. 2022;106(1):015308. doi:10.1103/PhysRevE.106.015308.
90. Schalkers MA, Möller M. On the importance of data encoding in quantum Boltzmann methods. Quantum Inf Process. 2024;23(1):20. doi:10.1007/s11128-023-04216-6.
91. Schalkers MA, Möller M. Momentum exchange method for quantum Boltzmann methods. Comput Fluids. 2024;285(1):106453. doi:10.1016/j.compfluid.2024.106453.
92. Georgescu CA, Möller M. Efficient and expressive boundary conditions in quantum lattice Boltzmann methods. arXiv:2606.01426. 2026.
93. Khan MI, Yao HD. A reproducible D3Q19 multiple-relaxation-time lattice Boltzmann benchmark and quantum-operator audit for forced wall-bounded flow simulations. Fluids. 2026;11(7):175. doi:10.3390/fluids11070175.
94. Grover L, Rudolph T. Creating superpositions that correspond to efficiently integrable probability distributions. arXiv:quant-ph/0208112. 2002.
95. Giovannetti V, Lloyd S, Maccone L. Quantum random access memory. Phys Rev Lett. 2008;100(16):160501. doi:10.1103/PhysRevLett.100.160501.

96. Aaronson S. Read the fine print. Nat Phys. 2015;11(4):291–3. doi:10.1038/nphys3272.
97. Huang HY, Kueng R, Preskill J. Predicting many properties of a quantum system from very few measurements. Nat Phys. 2020;16(10):1050–7. doi:10.1038/s41567-020-0932-7.
98. Succi S, Amati G, Bernaschi M, Falcucci G, Lauricella M, Montessori A. Towards exascale lattice Boltzmann computing. Comput Fluids. 2019;181(4):107–15. doi:10.1016/j.compfluid.2019.01.005.
99. Amati G, Succi S, Fanelli P, Krastev VK, Falcucci G. Projecting LBM performance on exascale class architectures: a tentative outlook. J Comput Sci. 2021;55(8):101447. doi:10.1016/j.jocs.2021.101447.
100. Falcucci G, Amati G, Fanelli P, Krastev VK, Polverino G, Porfiri M, et al. Extreme flow simulations reveal skeletal adaptations of deep-sea sponges. Nature. 2021;595(7868):537–41. doi:10.1038/s41586-021-03658-1.
101. Falcucci G, Amati G, Bella G, Facci AL, Krastev VK, Polverino G, et al. Adapting to the abyss: passive ventilation in the deep-sea glass sponge Euplectella aspergillum. Phys Rev Lett. 2024;132(20):208402. doi:10.1103/PhysRevLett.132.208402.
102. Sbragaglia M, Benzi R, Biferale L, Succi S, Sugiyama K, Toschi F. Generalized lattice Boltzmann method with multirange pseudopotential. Phys Rev E. 2007;75(2):026702. doi:10.1103/PhysRevE.75.026702.
103. Falcucci G, Ubertini S, Succi S. Lattice Boltzmann simulations of phase-separating flows at large density ratios: the case of doubly-attractive pseudo-potentials. Soft Matter. 2010;6(18):4357–65. doi:10.1039/C002974B.
104. Facci AL, Lauricella M, Succi S, Villani V, Falcucci G. Optimized modeling and design of a PCM-enhanced H2 storage. Energies. 2021;14(6):1554. doi:10.3390/en14061554.
105. McNamara GR, Zanetti G. Use of the Boltzmann equation to simulate lattice-gas automata. Phys Rev Lett. 1988;61(20):2332–5. doi:10.1103/PhysRevLett.61.2332.
106. Bhatnagar PL, Gross EP, Krook M. A model for collision processes in gases. I. Small amplitude processes in charged and neutral one-component systems. Phys Rev. 1954;94(3):511–25. doi:10.1103/PhysRev.94.511.
107. Qian YH, d'Humieres D, Lallemand P. Lattice BGK models for Navier–Stokes equation. Europhys Lett. 1992;17(6):479–84. doi:10.1209/0295-5075/17/6/001.
108. Guo Z, Shi B, Wang N. Lattice BGK model for incompressible Navier–Stokes equation. J Comput Phys. 2000;165(1):288–306. doi:10.1006/jcph.2000.6616.
109. Lallemand P, Luo LS. Theory of the lattice Boltzmann method: dispersion, dissipation, isotropy, Galilean invariance, and stability. Phys Rev E. 2000;61(6):6546–62. doi:10.1103/PhysRevE.61.6546.
110. Zou Q, He X. On pressure and velocity boundary conditions for the lattice Boltzmann BGK model. Phys Fluids. 1997;9(6):1591–8. doi:10.1063/1.869307.
111. Bouzidi M, Firdaouss M, Lallemand P. Momentum transfer of a Boltzmann-lattice fluid with boundaries. Phys Fluids. 2001;13(11):3452–9. doi:10.1063/1.1399290.
112. Mei R, Yu D, Shyy W, Luo LS. Force evaluation in the lattice Boltzmann method involving curved geometry. Phys Rev E. 2002;65(4):041203. doi:10.1103/PhysRevE.65.041203.
113. Colonius T, Lele SK. Computational aeroacoustics: progress on nonlinear problems of sound generation. Prog Aerosp Sci. 2004;40(6):345–416. doi:10.1016/j.paerosci.2004.09.001.
114. Buick JM, Greated CA, Campbell DM. Lattice BGK simulation of sound waves. Europhys Lett. 1998;43(3):235–40. doi:10.1209/epl/i1998-00346-7.
115. Shao W, Li J. Review of lattice Boltzmann method applied to computational aeroacoustics. Arch Acoust. 2019;44(2):215–38. doi:10.24425/aoa.2019.128486.
116. Sharma KV, Straka R, Tavares FW. Current status of lattice Boltzmann methods applied to aerodynamic, aeroacoustic, and thermal flows. Prog Aerosp Sci. 2020;115:100616. doi:10.1016/j.paerosci.2020.100616.
117. Bocanegra JA, Misale M, Borelli D. A systematic literature review on lattice Boltzmann method applied to acoustics. Eng Anal Bound Elem. 2024;158:405–29. doi:10.1016/j.enganabound.2023.11.007.
118. Vergnault E, Malaspinas O, Sagaut P. Noise source identification with the lattice Boltzmann method. J Acoust Soc Am. 2013;133(3):1293–305. doi:10.1121/1.4776181.
119. Vergnault E, Sagaut P. An adjoint-based lattice Boltzmann method for noise control problems. J Comput Phys. 2014;276:39–61. doi:10.1016/j.jcp.2014.07.027.

120. Ji C, Zhao D. Lattice Boltzmann investigation of acoustic damping mechanism and performance of an in-duct circular orifice. J Acoust Soc Am. 2014;135(6):3243–51. doi:10.1121/1.4876376.
121. Castro-Ávila E, Malgaretti P, Harting J, Muñoz JD. Lattice Boltzmann approach for acoustic manipulation. Phys Rev E. 2024;110(2):025304. doi:10.1103/PhysRevE.110.025304.
122. Lallemand P, Luo LS. Theory of the lattice Boltzmann method: acoustic and thermal properties in two and three dimensions. Phys Rev E. 2003;68(3):036706. doi:10.1103/PhysRevE.68.036706.
123. Marié S, Ricot D, Sagaut P. Comparison between lattice Boltzmann method and Navier–Stokes high order schemes for computational aeroacoustics. J Comput Phys. 2009;228(4):1056–70. doi:10.1016/j.jcp.2008.10.021.
124. Suss A, Mary I, Le Garrec T, Marié S. Comprehensive comparison between the lattice Boltzmann and Navier–Stokes methods for aerodynamic and aeroacoustic applications. Comput Fluids. 2023;257:105881. doi:10.1016/j.compfluid.2023.105881.
125. Ricot D, Marié S, Sagaut P, Bailly C. Lattice Boltzmann method with selective viscosity filter. J Comput Phys. 2009;228(12):4478–90. doi:10.1016/j.jcp.2009.03.030.
126. Brogi F, Malaspinas O, Chopard B, Bonadonna C. Hermite regularization of the lattice Boltzmann method for open source computational aeroacoustics. J Acoust Soc Am. 2017;142(4):2332–45. doi:10.1121/1.5006900.
127. Gendre F, Ricot D, Fritz G, Sagaut P. Grid refinement for aeroacoustics in the lattice Boltzmann method: a directional splitting approach. Phys Rev E. 2017;96(2):023311. doi:10.1103/PhysRevE.96.023311.
128. Astoul T, Wissocq G, Boussuge JF, Sengissen A, Sagaut P. Lattice Boltzmann method for computational aeroacoustics on non-uniform meshes: a direct grid coupling approach. J Comput Phys. 2021;447(7):110667. doi:10.1016/j.jcp.2021.110667.
129. Feuchter C. Direct aeroacoustic simulation with a cumulant lattice-Boltzmann model. Comput Fluids. 2021;224(3):104970. doi:10.1016/j.compfluid.2021.104970.
130. Bauer M, Eibl S, Godenschwager C, Kohl N, Kuron M, Rettinger C, et al. waLBerla: a block-structured high-performance framework for multiphysics simulations. Comput Math Appl. 2021;81(1):478–501. doi:10.1016/j.camwa.2020.01.007.
131. Qi J, Klimach H, Roller S. Implementation of the compact interpolation within the octree based lattice Boltzmann solver Musubi. Comput Math Appl. 2019;78(4):1131–41. doi:10.1016/j.camwa.2016.06.025.
132. Kam EWS, So RMC, Leung RCK. Lattice Boltzman method simulation of aeroacoustics and nonreflecting boundary conditions. AIAA J. 2007;45(7):1703–12. doi:10.2514/1.27632.
133. Junk M, Yang Z. Outflow boundary conditions for the lattice Boltzmann method. Prog Comput Fluid Dyn. 2008;8(1–4):38–48. doi:10.1504/PCFD.2008.018077.
134. Najafi-Yazdi A, Mongeau L. An absorbing boundary condition for the lattice Boltzmann method based on the perfectly matched layer. Comput Fluids. 2012;68(1):203–18. doi:10.1016/j.compfluid.2012.07.017.
135. Xu H, Sagaut P. Analysis of the absorbing layers for the weakly-compressible lattice Boltzmann methods. J Comput Phys. 2013;245(13):14–42. doi:10.1016/j.jcp.2013.02.051.
136. Farassat F. Derivation of formulations 1 and 1A of farassat. Hampton, VA, USA: NASA Langley Research Center; 2007.
137. Najafi-Yazdi A, Brès GA, Mongeau L. An acoustic analogy formulation for moving sources in uniformly moving media. Proc Royal Soc A Math Phys Eng Sci. 2010;467(2125):144–65. doi:10.1098/rspa.2010.0172.
138. Baretter A, Godard B, Joseph P, Roussette O, Romanò F, Barrier R, et al. Experimental and numerical analysis of a compressor stage under flow distortion. Int J Turbomach, Propuls Power. 2021;6(4):43. doi:10.3390/ijtpp6040043.
139. Elhawary MA, Romanò F, Loiseau JC, Dazin A. Machine learning for optimal flow control in an axial compressor. Eur Phys J E. 2023;46(4):28. doi:10.1140/epje/s10189-023-00284-9.
140. Schoder S, Junger C, Kaltenbacher M. Computational aeroacoustics of the EAA benchmark case of an axial fan. Acta Acustica. 2020;4(5):22. doi:10.1051/aacus/2020021.
141. Cantos S, Zhou P, Wu H, Ma Z, Chen W, Zhong S, et al. Aerodynamics and aeroacoustics of ducted propellers: a study on the design and geometry effects. Phys Fluids. 2024;36(3):035116. doi:10.1063/5.0191323.

142. Astley RJ, Sugimoto R, Mustafi P. Computational aero-acoustics for fan duct propagation and radiation. Current status and application to turbofan liner optimisation. J Sound Vib. 2011;330(16):3832–45. doi:10.1016/j.jsv.2011.03.022.
143. Kierkegaard A, Boij S, Efraimsson G. A frequency domain linearized Navier–Stokes equations approach to acoustic propagation in flow ducts with sharp edges. J Acoust Soc Am. 2010;127(2):710–9. doi:10.1121/1.3273899.
144. Kadowaki T, Nishimori H. Quantum annealing in the transverse Ising model. Phys Rev E. 1998;58(5):5355–63. doi:10.1103/PhysRevE.58.5355.
145. Lucas A. Ising formulations of many NP problems. Front Phys. 2014;2:5. doi:10.3389/fphy.2014.00005.
146. Farhi E, Goldstone J, Gutmann S. A quantum approximate optimization algorithm. arXiv:1411.4028. 2014.
147. Childs AM, Wiebe N. Hamiltonian simulation using linear combinations of unitary operations. Quantum Inf Comput. 2012;12(11–12):901–24. doi:10.26421/QIC12.11-12-1.
148. Tissot G, Billard R, Gabard G. Optimal cavity shape design for acoustic liners using Helmholtz equation with visco-thermal losses. J Comput Phys. 2020;402(4):109048. doi:10.1016/j.jcp.2019.109048.
149. Berry DW. High-order quantum algorithm for solving linear differential equations. J Phys A Math Theor. 2014;47(10):105301. doi:10.1088/1751-8113/47/10/105301.
150. Berry DW, Childs AM, Ostrander A, Wang G. Quantum algorithm for linear differential equations with exponentially improved dependence on precision. Commun Math Phys. 2017;356(3):1057–81. doi:10.1007/s00220-017-3002-y.
151. Childs AM, Liu JP. Quantum spectral methods for differential equations. Commun Math Phys. 2020;375(2):1427–57. doi:10.1007/s00220-020-03699-z.
152. Childs AM, Liu JP, Ostrander A. High-precision quantum algorithms for partial differential equations. Quantum. 2021;5:574. doi:10.22331/q-2021-11-10-574.
153. d'Humières D, Ginzburg I, Krafczyk M, Lallemand P, Luo LS. Multiple-relaxation-time lattice Boltzmann models in three dimensions. Philos Trans Royal Soc London Ser A Math, Phys Eng Sci. 2002;360(1792):437–51. doi:10.1098/rsta.2001.0955.
154. Zhuo C, Sagaut P. Acoustic multipole sources for the regularized lattice Boltzmann method: comparison with multiple-relaxation-time models in the inviscid limit. Phys Rev E. 2017;95(6):063301. doi:10.1103/PhysRevE.95.063301.
155. Xiao Y, Fang K, Zhong K, Lu J. A lattice Boltzmann method with source term for acoustic problems. J Acoust Soc Am. 2025;158(1):663–83. doi:10.1121/10.0037189.
156. Sanavio C, Simon WA, Ralli A, Love P, Succi S. Carleman-lattice-Boltzmann quantum circuit with matrix access oracles. Phys Fluids. 2025;37(3):037123. doi:10.1063/5.0254588.
157. Krovi H. Improved quantum algorithms for linear and nonlinear differential equations. Quantum. 2023;7:913. doi:10.22331/q-2023-02-02-913.
158. Costa PCS, An D, Sanders YR, Su Y, Babbush R, Berry DW. Optimal scaling quantum linear-systems solver via discrete adiabatic theorem. PRX Quantum. 2022;3(4):040303. doi:10.1103/PRXQuantum.3.040303.
159. Liu JP, Kolden HØ, Krovi HK, Loureiro NF, Trivisa K, Childs AM. Efficient quantum algorithm for dissipative nonlinear differential equations. Proc Natl Acad Sci U S A. 2021;118(35):e2026805118. doi:10.1073/pnas.2026805118.
160. Bastida Zamora AD, Budinski L, Lahtinen V, Sagaut P. Quantum lattice Boltzmann method for several time steps: a local Carleman linearization algorithm. Phys Rev E. 2026;113(3):035307. doi:10.1103/kbx3-c35d.
161. Berry DW, Childs AM, Cleve R, Kothari R, Somma RD. Simulating Hamiltonian dynamics with a truncated Taylor series. Phys Rev Lett. 2015;114(9):090502. doi:10.1103/PhysRevLett.114.090502.
162. Low GH, Chuang IL. Hamiltonian simulation by qubitization. Quantum. 2019;3:163. doi:10.22331/q-2019-07-12-163.
163. An D, Liu JP, Lin L. Linear combination of Hamiltonian simulation for nonunitary dynamics with optimal state preparation cost. Phys Rev Lett. 2023;131(15):150603. doi:10.1103/PhysRevLett.131.150603.
164. Fang D, Lin L, Tong Y. Time-marching based quantum solvers for time-dependent linear differential equations. Quantum. 2023;7:955. doi:10.22331/q-2023-03-20-955.

165. Brassard G, Høyer P, Mosca M, Tapp A. Quantum amplitude amplification and estimation. arXiv:quant-ph/0005055. 2000.
166. Suzuki Y, Uno S, Raymond R, Tanaka T, Onodera T, Yamamoto N. Amplitude estimation without phase estimation. Quantum Inf Process. 2020;19(2):75. doi:10.1007/s11128-019-2565-2.
167. Grinko D, Gacon J, Zoufal C, Woerner S. Iterative quantum amplitude estimation. npj Quantum Inf. 2021;7(1):52. doi:10.1038/s41534-021-00379-1.
168. Beverland ME, Murali P, Troyer M, Svore KM, Hoefler T, Kliuchnikov V, et al. Assessing requirements to scale to practical quantum advantage. arXiv:2211.07629. 2022.
169. Brunton SL, Noack BR, Koumoutsakos P. Machine learning for fluid mechanics. Ann Rev Fluid Mech. 2020;52(1):477–508. doi:10.1146/annurev-fluid-010719-060214.
170. Bae HJ, Koumoutsakos P. Scientific multi-agent reinforcement learning for wall-models of turbulent flows. Nat Commun. 2022;13(1):1443. doi:10.1038/s41467-022-28957-7.
171. Novati G, de Laroussilhe HL, Koumoutsakos P. Automating turbulence modelling by multi-agent reinforcement learning. Nat Mach Intell. 2021;3(1):87–96. doi:10.1038/s42256-020-00272-0.